

University of Nevada, Reno

**Electrocatalytic CO<sub>2</sub> Reduction**  
**by Self-Assembled Monolayers of Metal Porphyrins**

A thesis submitted in partial fulfillment of the  
requirements for the degree of Master of Science in  
Chemistry

by

Jason A. Mennel

Dr. Christopher J. Barile/Thesis Advisor

May 2020

**Copyright by Jason A. Mennel 2020**

**All Rights Reserved**

THE GRADUATE SCHOOL

We recommend that the thesis  
prepared under our supervision by

JASON MENNEL

entitled

Electrocatalytic CO<sub>2</sub> Reduction by Self-Assembled  
Monolayers of Metal Porphyrins

be accepted in partial fulfillment of the  
requirements for the degree of

MASTER OF SCIENCE

Christopher Barile, Ph.D.  
*Advisor*

Brian J. Frost, Ph.D.  
*Committee Member*

Dev Chidambaram, Ph.D.  
*Graduate School Representative*

David W. Zeh, Ph.D., Dean  
*Graduate School*

May, 2020

**Abstract**

The main issue hindering the successful utilization of CO<sub>2</sub> electroreduction processes in industry is the lack of selective, durable, and efficient catalysts. We design a new heterogenous molecular architecture for CO<sub>2</sub> electrocatalysts by attaching alkyne-terminated metal (Fe, Co) porphyrins via click chemistry to azide-terminated alkyl phosphate self-assembled monolayers (SAMs) on ITO and FTO electrodes. The electrochemistry of these CO<sub>2</sub> reduction systems is studied using cyclic voltammetry and chronoamperometry, and products are quantified through NMR and GC techniques. Additionally, AFM is used to characterize the morphology of the electrode surfaces. Experiments show that CO<sub>2</sub> reduction is highly sensitive to the surrounding environment and choices of electrode, SAM length, metal porphyrin or external potential greatly affect reduction products. Our results indicate that FTO is a more electrochemically stable substrate and an intermediate length SAM such as an 11 carbon chain length optimize CO<sub>2</sub> reduction conditions towards formate and carbon monoxide with our metal porphyrins. The chemical tunability of SAMs allows for a high degree of control over the surface modification of CO<sub>2</sub> electrocatalysts, potentially enabling the design of superior catalysts.

**Table of Contents**

Acknowledgements	iii
List of Figures	iv-vi
Chapter 1: Introduction	1-3
References	3-4
Chapter 2: Electrocatalytic CO <sub>2</sub> Reduction by Self-Assembled Monolayers of Metal Porphyrins	5-40
Introduction	5-6
Materials and Methods	6-18
Results and Discussion	18-37
Conclusion	37-38
References	38-40

**Acknowledgements**

Acknowledgement is made to the donors of The American Chemical Society Petroleum Research Fund for partial support of this research. I thank Research and Innovation at the University of Nevada, Reno for partial support of this research. I acknowledge the Shared Instrumentation Laboratory in the Department of Chemistry at the University of Nevada, Reno.

**List of Figures**

Figure 1: $^1\text{H}$ NMR spectrum in $\text{CDCl}_3$ of 5-(4-(3-hydroxy-3-methyl-1-butynylphenyl)-10,15,20-triphenylporphyrin. The peaks at 1.16 ppm and 2.38 ppm are due to residual propionic acid used as the solvent in the synthesis	8
Figure 2: $^1\text{H}$ NMR spectrum in $\text{CDCl}_3$ of 5-(4-ethynylphenyl)-10,15,20-triphenylporphyrin	9
Figure 3: UV-visible absorbance spectrum of the clickable porphyrin without metal (black line), the clickable Fe porphyrin (red line), and the clickable Co porphyrin (blue line) in dichloromethane. The concentrations of the porphyrin were 310 $\mu\text{M}$ , 72 $\mu\text{M}$ , and 190 $\mu\text{M}$ , respectively	10
Figure 4: $^1\text{H}$ NMR spectrum in $\text{CDCl}_3$ of 11-azido-1-undecanol	11
Figure 5: $^1\text{H}$ NMR spectrum in $\text{CDCl}_3$ of 11-azidoundecylphosphonic acid. The singlet at 2.17 ppm is due to residual acetone	12
Figure 6: $^1\text{H}$ NMR spectrum in $\text{CDCl}_3$ of 5-azido-1-pentanol	14
Figure 7: $^1\text{H}$ NMR spectrum in $\text{CDCl}_3$ of 16-azido-1-hexadecanol	14
Figure 8: $^1\text{H}$ NMR spectrum in $\text{CDCl}_3$ of 5-azidopentylidihydrogen phosphate	15
Figure 9: Schematic of the attachment of porphyrin catalysts to Au or ITO electrodes using azide-alkyne click chemistry	19
Figure 10: Linear sweep voltammograms of FeTPP-modified Au electrodes at 10 mV/s in a pH 7 phosphate buffer sparged with $\text{N}_2$ (black line) and $\text{O}_2$ (red line)	20
Figure 11: AFM images of unmodified Au (a) and CoTPP-modified Au (b) surfaces	21
Figure 12: Cyclic voltammograms of unmodified ITO (black line) and ITO surfaces modified with SAM (red line), $\text{H}_2\text{TPP}$ (blue line), and FeTPP (green line) at 100 mV/s in $\text{CO}_2$ -sparged 100 mM $\text{NaHCO}_3$	22
Figure 13: Cyclic voltammograms of unmodified ITO (black line) and ITO surfaces modified with SAM (red line), $\text{H}_2\text{TPP}$ (blue line), and FeTPP (green line) at 50 mV/s in 1 mM $\text{K}_3\text{Fe}(\text{CN})_6$ with 100 mM $\text{NaCl}$	23
Figure 14: AFM images of unmodified ITO (a, b) and CoTPP-modified ITO (c, d) surfaces	24
Figure 15: Cyclic voltammograms of ITO electrodes modified with FeTPP (a)	26

and CoTPP (b) in 100 mM NaHCO<sub>3</sub> sparged with N<sub>2</sub> (black lines) and CO<sub>2</sub> (red lines) at 10 mV/s

Figure 16: Cyclic voltammograms of Cu foil in 100 mM NaHCO<sub>3</sub> sparged with CO<sub>2</sub> (red line) and N<sub>2</sub> (black line) at 10 mV/s 26

Figure 17: Cyclic voltammograms of unmodified ITO (black lines) and ITO modified with SAM (red lines) and H<sub>2</sub>TPP (blue lines) in 100 mM NaHCO<sub>3</sub> sparged with CO<sub>2</sub> (a) and N<sub>2</sub> (b) at 10 mV/s 27

Figure 18: Chronoamperometry at -1.6 V of unmodified ITO (black line) and ITO modified with CoTPP (blue line) in 100 mM NaHCO<sub>3</sub> sparged with CO<sub>2</sub> (a) and faradaic efficiencies for each surface (b) 28

Figure 19: Gas chromatograms of the CO peak formed after chronoamperometry at -1.6 V for 1 hour using an unmodified ITO electrode (blue line) and ITO modified with CoTPP (black line) and FeTPP (red line). The green line represents an air sample 28

Figure 20: Common reduction potentials for the components indium and tin in ITO substrate 29

Figure 21: A comparison between the chronoamperometry of bare ITO and bare FTO at -1.6V in 100 mM NaHCO<sub>3</sub> sparged with CO<sub>2</sub> (a) and photographs of substrates after voltammetry experiments starting at 0 V sweeping to different negative voltages between ITO and FTO substrates (b) 30

Figure 22: Cyclic voltammogram of FTO electrodes modified with FeTPP and CoTPP porphyrins in 100 mM NaHCO<sub>3</sub> sparged with CO<sub>2</sub> (a) and cyclic voltammogram (b) of unmodified FTO (black line) and FTO surfaces modified with FeTPP (red line) and CoTPP (blue line) at 50 mV/s in 1 mM K<sub>3</sub>Fe(CN)<sub>6</sub> with 100 mM NaCl 31

Figure 23: Faradaic efficiencies at three voltages for C<sub>11</sub> SAM (a), C<sub>5</sub> SAM (b) and C<sub>16</sub> SAM (c) 32

Figure 24: Mechanism for electrocatalytic CO<sub>2</sub> reduction 33

Figure 25: Mole comparisons of different porphyrin modified surfaces (a,b) and charge comparisons of each porphyrin modified surface (c,d) 34

Figure 26: Optical microscope images at medium objective for porphyrin modified FTO surfaces after experiment at -1.2 V (a), -1.4 V (b) and -1.6 V (c) 35

Figure 27: Faradaic efficiencies at three voltages for C<sub>11</sub> SAM (a) and C<sub>5</sub> SAM (b) 36

Figure 28: Combined Faradaic efficiencies for select surfaces

37

## Chapter 1: Introduction

According to the U.S. Environmental Protection Agency, the average American produces about 4.51 pounds of trash per day.[1] Per year, that translates to roughly 0.8 tons. In contrast, the average American uses transportation or appliances that emit 16.2 tons of CO<sub>2</sub> per year.[2] These numbers still pale in comparison to the emissions from industry, about 6.7 billion metric tons of CO<sub>2</sub> in 2018 and accounting for almost a quarter of emissions from the entire United States.[3] Over the decades it has become apparent the effects this accumulation has had on our way of life, from changing climate patterns, to acidification of the oceans and ecological affects, to adverse personal health issues. These dramatic changes should alert us to the severity with which we need to reduce our carbon emissions. It is also useful to know that a portion of CO<sub>2</sub> emissions from industry comes from the production of commodity chemicals such as alcohols, olefins and syngas,[4] meaning if we can utilize CO<sub>2</sub> to manufacture these products, we create a negative emission loop and still generate valuable chemicals once derived from fossil fuels. Several approaches exist like more efficient energy appliances or carbon capture and sequestration, but CO<sub>2</sub> conversion, part of a negative emissions approach, could be the 21<sup>st</sup> century solution we need to a major 21<sup>st</sup> century problem.

One carbon capture technology, geological injection, has shown success so far in reducing amounts of CO<sub>2</sub> in air, however long-term storage effects like potential leaks are not known.[5] A plant can be designed to actively capture and store CO<sub>2</sub>, usually built next to the source of CO<sub>2</sub> generation, the largest plant in the world being the Century Plant built in West Texas.[6] This method is useful for enhanced oil recovery. Both methods however treat CO<sub>2</sub> as a waste product instead of a useful intermediate chemical. Molecular

conversion of CO<sub>2</sub> is a popular alternative to carbon capture technologies and the utility of reduced products like formate, syngas, methane, methanol and carbon monoxide can be vital towards chemical manufacturing.[7,8] Molecular conversion can proceed via electrochemical, photochemical, biological and inorganic processes.[9] Electrochemical conversion is by far the most promising technology due to the benefits of being paired with renewable energy sources such as wind and solar and low cost of equipment and safe operating conditions.[10] Furthermore, the system can be easily controlled by varying the external potential, electrolytes or catalysts.[10] Even among electrochemical reduction techniques, there are significant approaches to facilitate effective conversion.

While there are successful homogeneous electroreduction catalysts[11-13] that benefit from high product selectivity and simple experimental design, heterogeneous systems have advantages such as using catalysts with low toxicity, high durability, and ease of separation of products.[14] Another major benefit to heterogeneous catalysts is while selectivity may be low, the structure-reactivity relationships are easier to study and therefore allow for greater optimization towards selective product generation.[14] Many electrocatalysts have been studied from bulk metals, to metallic hybrids, metal oxides and nanomaterials to molecular catalysts.[15] An effective catalyst must be selective towards a single reduction product, must produce high efficiencies of that product, and must be durable to reduce hundreds of thousands of CO<sub>2</sub> molecules. While many catalysts have had success in one of these categories, most still lack dominance in all three. Molecular catalysts are opportune when considering metal usage is minimized and turn over number (TON) and turnover frequency (TOF) are high.[9] Some examples of molecular catalysts are covalent organic frameworks (COF), metal organic frameworks (MOF) and

independent molecular catalysts like porphyrins. MOF's have seen a rise in success due to the tunability of the system[16], but due to the inherent nature of a MOF the organic components are all linked together and lack the control of a system where catalysts act independent of each other. Porphyrins are the most studied molecular catalysts for CO<sub>2</sub> reduction and have mild success in typically homogeneous media where they are easier to separate and reuse but lack tunability.[17] Using metal porphyrins in a heterogeneous system could allow for ease of separation of products coupled with a greater analysis of structure-reactivity that subsequently allows for further optimization than analogous homogeneous systems. Compared to complicated binding techniques that adhere molecular catalysts to an electrode surface, self-assembled monolayers (SAMs) offer simple attachment and easier surface analysis.[18] The focus of this thesis is in analyzing various SAM modified surfaces for porphyrin attachment towards electrocatalytic CO<sub>2</sub> reduction and assessing the tunability of catalysts towards reduction products.

## References

- [1] Facts and Figures about Materials, Waste and Recycling, United States Environmental Protection Agency, <https://www.epa.gov/facts-and-figures-about-materials-waste-and-recycling/national-overview-facts-and-figures-materials#main-content>, (accessed April 30, 2020)
- [2] H. Ritchie, **Where in the World do People Emit the Most CO<sub>2</sub>?**, Our World in Data, 2019
- [3] Sources of Greenhouse Gas Emissions, United States Environmental Protection Agency, <https://www.epa.gov/ghgemissions/sources-greenhouse-gas-emissions>, (accessed April 30, 2020)
- [4] De Luna, P.; Hahn, C.; Higgins, D.; Jaffer, S. A.; Jaramillo, T. F.; Sargent, E. H. **What Would It Take for Renewably Powered Electrosynthesis to Displace Petrochemical Processes?** *Science*, 2019, *364* (6438). <https://doi.org/10.1126/science.aav3506>
- [5] A.B. Klass, E.J. Wilson, **Climate Change and Carbon Sequestration: Assessing a Liability Regime for Long-term Storage of Carbon Dioxide**, (2008)
- [6] What are the top carbon capture and storage projects around the world?, NS Energy, <https://www.nsenergybusiness.com/features/top-carbon-capture-storage-projects/>, (accessed April 30, 2020)

- [7] A. Goeppert, M. Czaun, J.-P. Jones, G.K. Surya Prakash, G.A. Olah, **Recycling of carbon dioxide to methanol and derived products — closing the loop** Chem.Soc. Rev., 43 (2014), 7995–8048
- [8] D.T. Whipple, P.J.A. Kenis, **Prospects of CO<sub>2</sub> Utilization via Direct Heterogeneous Electrochemical Reduction** J. Phys. Chem. Lett., 1 (2010) 3451–3458
- [9] Kumar, B.; Brian, J. P.; Atla, V.; Kumari, S.; Bertram, K. A.; White, R. T.; Spurgeon, J. M. **New Trends in the Development of Heterogeneous Catalysts for Electrochemical CO<sub>2</sub> Reduction** Catal. Today, 270 (2016), 19–30
- [10] Long, C.; Li, X.; Guo, J.; Shi, Y.; Liu, S.; Tang, Z. **Electrochemical Reduction of CO<sub>2</sub> over Heterogeneous Catalysts in Aqueous Solution: Recent Progress and Perspectives** Small Methods, (2018), 1800369
- [11] Smieja, J. M.; Sampson, M. D.; Grice, K. A.; Benson, E. E.; Froehlich, J. D.; Kubiak, C. P. **Manganese as a Substitute for Rhenium in CO<sub>2</sub> Reduction Catalysts: The Importance of Acids** Inorg. Chem., 52 (2013), 2484–2491
- [12] Margarit, C. G.; Asimow, N. G.; Costentin, C.; Nocera, D. G. **Tertiary Amine-Assisted Electroreduction of Carbon Dioxide to Formate Catalyzed by Iron Tetraphenylporphyrin** ACS Energy Lett., 5 (2020), 72–78
- [13] Seshadri, G.; Lin, C.; Bocarsly, A. B. **A New Homogeneous Electrocatalyst for the Reduction of Carbon Dioxide to Methanol at Low Overpotential** J. Electroanal. Chem., 372 (1994), 145–150
- [14] Francke, R.; Schille, B.; Roemelt, M. **Homogeneously Catalyzed Electroreduction of Carbon Dioxide - Methods, Mechanisms, and Catalysts** Chem. Rev., 118 (2018), 4631–4701
- [15] Kuhl, K. P.; Hatsukade, T.; Cave, E. R.; Abram, D. N.; Kibsgaard, J.; Jaramillo, T. F. **Electrocatalytic Conversion of Carbon Dioxide to Methane and Methanol on Transition Metal Surfaces** J. Am. Chem. Soc., 136 (2014), 14107–14113
- [16] Kornienko, N.; Zhao, Y.; Kley, C. S.; Zhu, C.; Kim, D.; Lin, S.; Chang, C. J.; Yaghi, O. M.; Yang, P. **Metal-Organic Frameworks for Electrocatalytic Reduction of Carbon Dioxide** J. Am. Chem. Soc., 137 (2015), 14129–14135
- [17] B.-X. Dong, S.-L. Qian, F.-Y. Bu, Y.-C. Wu, L.-G. Feng, Y.-L. Teng, W.-L. Liu, Z.-W. Li, **Electrochemical Reduction of CO<sub>2</sub> to CO by a Heterogeneous Catalyst of Fe-Porphyrin-Based Metal-Organic Framework** ACS Appl. Energy Mater., 1 (2018), 4662-4669
- [18] S.N. Supakul, C.J. Barile, **Membrane-modified Metal Triazole Complexes for the Electrocatalytic Reduction of Oxygen and Carbon Dioxide** Front. Chem. (Lausanne, Switz.), 6 (2018), 543

## **Chapter 2: Electrocatalytic CO<sub>2</sub> Reduction by Self-Assembled Monolayers of Metal Porphyrins**

### **1. Introduction**

With CO<sub>2</sub> levels surpassing 410 ppm in 2019[1], it is increasingly more urgent to facilitate carbon neutral and carbon capture practices. Electrochemical reduction of CO<sub>2</sub> has not just the advantage of negating carbon emissions, but also of converting the CO<sub>2</sub> in the atmosphere into useful commodity chemicals. Ever since electrochemical reduction of CO<sub>2</sub> research began with Hori et al.,[2, 3] many catalysts have been realized for active electroreduction. Metals,[4-7] metal oxides,[8, 9] and a multitude of molecular compounds have been found to reduce CO<sub>2</sub>. [10] Despite the large number of catalysts studied, there is not yet a single catalyst that possesses the selectivity, efficiency, and durability needed for practical industrial applications.

For molecular catalysts, CO<sub>2</sub> reduction is frequently performed using carbon electrodes that contain a binder like Nafion to attach the catalyst to the electrode. Using a dropcast method, a porous multilayer catalyst architecture is formed, which is beneficial for high current density applications but complicates electrode surface structure.[11] The binder in the electrode matrix also affects the rate of proton transfer and CO<sub>2</sub> diffusion to the catalyst.

The attachment of catalysts to self-assembled monolayers (SAMs) is an alternative to multilayer architectures that does not require a binder. Furthermore, SAMs simplify analysis of the activity of molecular CO<sub>2</sub> catalysts because only a monolayer of catalyst is

present. By using SAMs containing a mixture of surface functionalities, the surface coverage of the catalyst can be precisely tuned.[12] This ability allows for greater control of reaction dynamics. For example, by changing the intermolecular spacing of catalysts on the electrode, the extent of dimerization can be modulated.[13] Additionally, the SAM chain length can be altered to adjust electron transfer rate to the appended catalyst.[14] The electron transfer kinetics can in turn alter the mechanism of catalysis.[15]

Porphyrins and related macrocycles are common molecular catalysts for electrochemical CO<sub>2</sub> reduction. Previous research has shown high selectivity for CO, formate, and methane depending upon the sterics, electronics, and metal present in the porphyrin. Dong et al. demonstrated a 91% Faradaic efficiency towards CO using a Fe porphyrin on a carbon substrate.[16] Chen et al. demonstrated selectivity towards formate using an N5 pentadentate complex[17] while Weng and coworkers utilized a Cu porphyrin that possessed a 47% Faradaic efficiency towards methane.[18]

In this work, we describe Fe and Co porphyrin electrocatalysts that are active towards CO<sub>2</sub> reduction using azide-alkyne chemistry to append the catalysts to indium tin oxide (ITO) and fluorine tin oxide (FTO) working electrodes. To attach the porphyrins to the electrodes, we react alkyne-modified porphyrins with azide-terminated phosphate SAMs onto the substrates. This platform combines the tunability of SAM surface chemistry with molecular CO<sub>2</sub> electrocatalysts, which establishes a potential framework for greater control over catalyst performance.

## **2. Materials and methods**

### *2.1. General Procedures*

All starting materials and electrolyte chemicals were obtained from commercially available sources and used without further purification. The alkyne porphyrin (H<sub>2</sub>TPP) ligand and the azide-terminated phosphates were synthesized following procedures described in the “Synthetic Procedures” section in the Supplementary Material. Electrochemical studies were carried out using a VSP-300 Biologic potentiostat. For electrochemical studies, a three-electrode system was used with a Pt counter electrode, a Ag/AgCl reference electrode (3 M KCl, eDAQ, Inc.), and a Au, ITO or FTO working electrode. Au working electrodes were prepared from recordable CDs according to a literature procedure.[19] ITO and FTO working electrodes were ordered from Xin Yan, Inc. (10 Ω/sq). ITO and FTO substrates were cleaned via sonication in Extran followed by sonication in isopropanol for 5 minutes each. All experiments were carried out at a temperature of (25 ± 1) °C.

## 2.2. Synthetic Procedures

Dichloromethane (DCM), tetrahydrofuran (THF), dimethylformamide (DMF), toluene, and propionic acid, were of reagent grade and used without further purification. Column chromatography was performed using 230-400 mesh silica gel. NMR spectra were obtained using a Varian 400 MHz NMR Spectrometer in the Shared Instrument Laboratory (SIL) in the Department of Chemistry at the University of Nevada, Reno (UNR). <sup>1</sup>H NMR spectra were recorded in CDCl<sub>3</sub> and referenced to the residual protio solvent peak at 7.26 parts per million (ppm). Chemical shifts (δ) and coupling constants (J) are reported in ppm and hertz (Hz), respectively.

### 2.2.1. Synthesis of 5-(4-(3-hydroxy-3-methyl-1-butynylphenyl)-10,15,20-triphenylporphyrin

This porphyrin was synthesized following a previously published procedure.[20] A solution of 4-(3-hydroxy-3-methyl-1-butynyl)-benzaldehyde (1.9 g, 10 mmol) and benzaldehyde (3.05 mL, 30 mmol) in propionic acid (100 mL) was heated to reflux, and pyrrole (2.75 mL, 40 mmol) was added dropwise over 5 min while sparging with N<sub>2</sub>. After sparging with N<sub>2</sub>, the solution was stirred at reflux under air for 3 hours after which the solvent was removed *in vacuo*, yielding a mixture of tetraaryl porphyrins. The title compound was collected as the second fraction by silica-gel column chromatography using dichloromethane as eluent. After removal of solvent by vacuum, the product was obtained as a dark purple solid (0.351 g, 5.1% yield based on pyrrole). <sup>1</sup>H NMR (400 MHz in CDCl<sub>3</sub>): δ 8.81-8.87 (m, 8H, pyrrole), 8.16-8.23 (m, 8H, Ph-2,6 and Ph'-2,6), 7.82 (d, 2H, Ph'-3,5, J = 8.1 Hz), 7.77 (m, 9H, Ph-3,4,5), 1.77 (s, 6H), -2.78 (s, 2H, N-H).

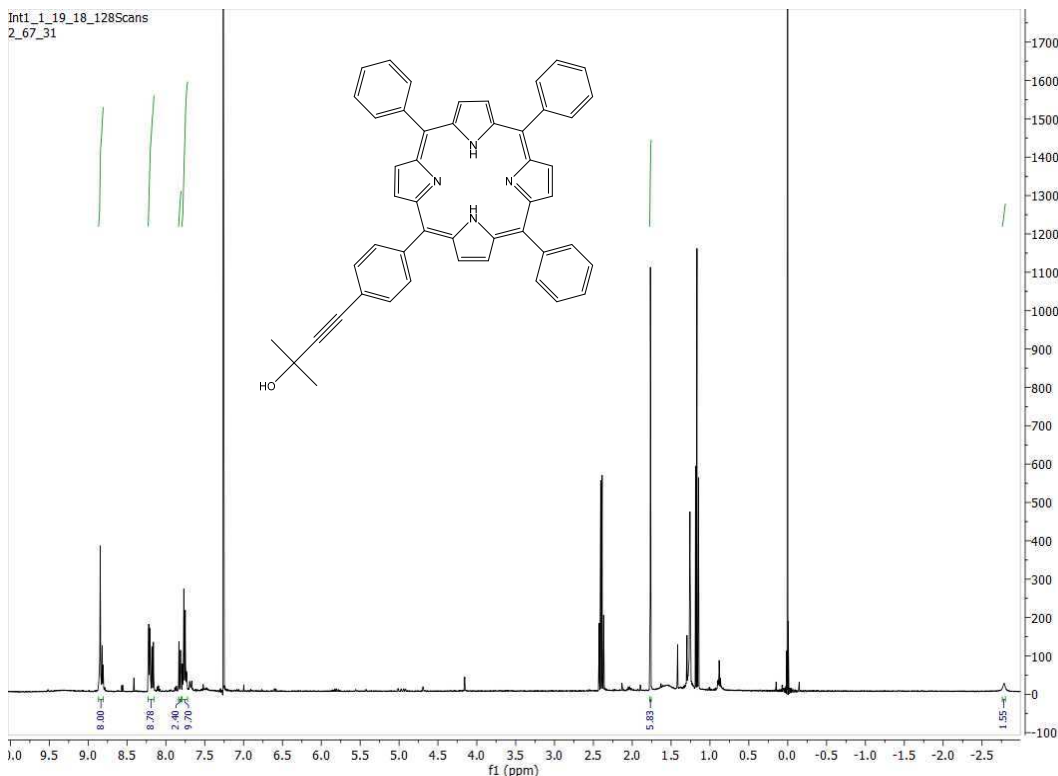


**Figure 1:** <sup>1</sup>H NMR spectrum of 5-(4-(3-hydroxy-3-methyl-1-butynyl)phenyl)-10,15,20-triphenylporphyrin. The peaks at 1.16 ppm and 2.38 ppm are due to residual propionic acid used as the solvent in the synthesis.

### 2.2.2. Synthesis of 5-(4-ethynylphenyl)-10,15,20-triphenylporphyrin ( $H_2TPP$ )

5-(4-(3-hydroxy-3-methyl-1-butynyl)phenyl)-10,15,20-triphenylporphyrin (0.106 g, 0.15 mmol) was stirred with KOH (2.0 g, 36 mmol) in refluxing toluene under  $N_2$  for 4 hours to remove the ethynyl protecting group. This solution was then washed with water, dried with  $Na_2SO_4$ , and the solvent was removed *in vacuo*. The mono-ethynyl porphyrin was not purified any further and resulted in a dark purple red solid (0.060 g, 61% yield).  $^1H$  NMR (400 MHz in  $CDCl_3$ )  $\delta$  8.76-8.86 (m, 8H, pyrrole), 8.15-8.21 (m, 8H, Ph-2,6 and Ph'-2,6), 7.87 (d, 2H, Ph'-3,5,  $J=8.3$  Hz), 7.75 (m, 9H, Ph-3,4,5), 3.30 (s, 1H), -2.80 (s, 2H, N-H).

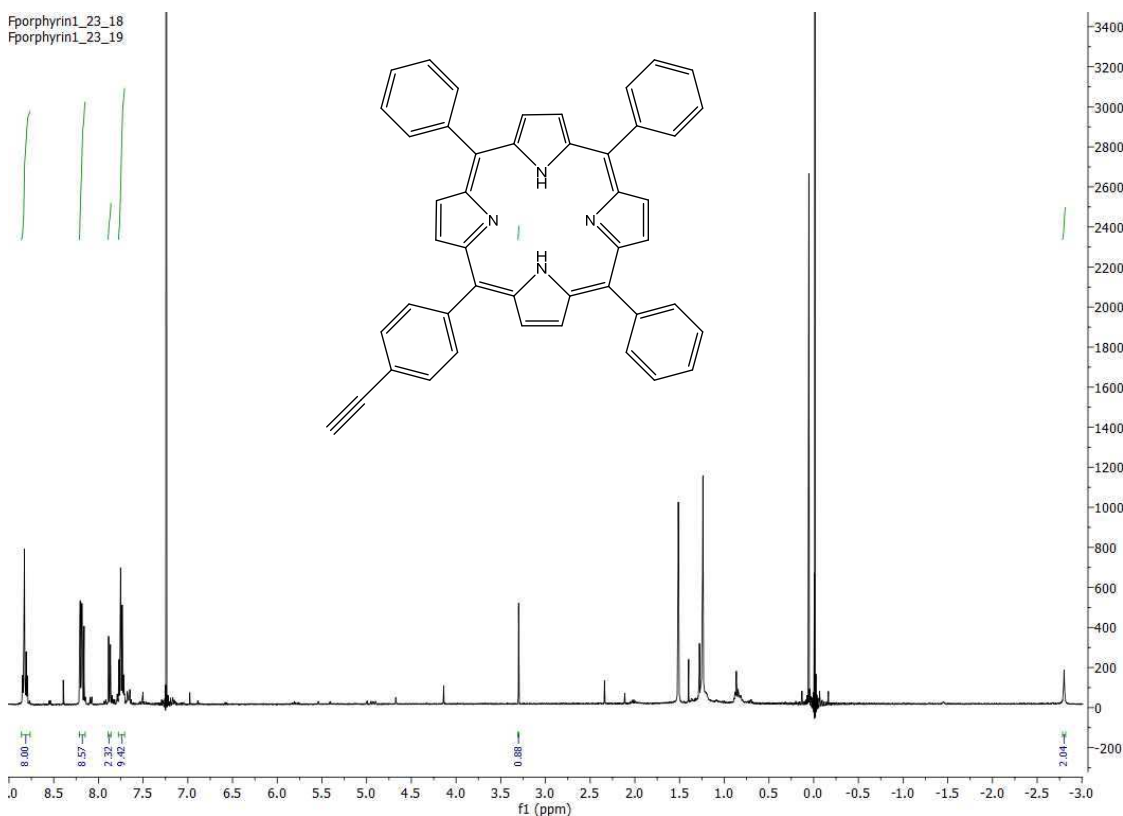


**Figure 2:**  $^1H$  NMR spectrum of 5-(4-ethynylphenyl)-10,15,20-triphenylporphyrin.

2.2.3. *Synthesis of 5-(4-ethynylphenyl)-10,15,20-triphenylporphyrinato chloro Fe<sup>3+</sup> (FeTPP)*

5-(4-ethynylphenyl)-10,15,20-triphenylporphyrin (0.030 g, 0.047 mmol) was stirred at reflux in DMF (10 mL) while FeCl<sub>2</sub> (0.080 g, 0.64 mmol) was added under N<sub>2</sub>. The solution was then refluxed under air for 1 h. After cooling to room temperature, H<sub>2</sub>O (20 mL) was added to the reaction mixture, and the resulting purple powder was collected by filtration. The title compound (17.8 mg, 52.4% yield) was not purified further.

2.2.4. *Synthesis of 5-(4-ethynylphenyl)-10,15,20-triphenylporphyrinato chloro Co<sup>2+</sup> (CoTPP).*

This synthesis followed the same procedure as the Fe analogue using 5-(4-ethynylphenyl)-10,15,20-triphenylporphyrin (0.050 g, 0.078 mmol) resulting in Co-ethynylTPPCl (0.042 g, 73% yield).

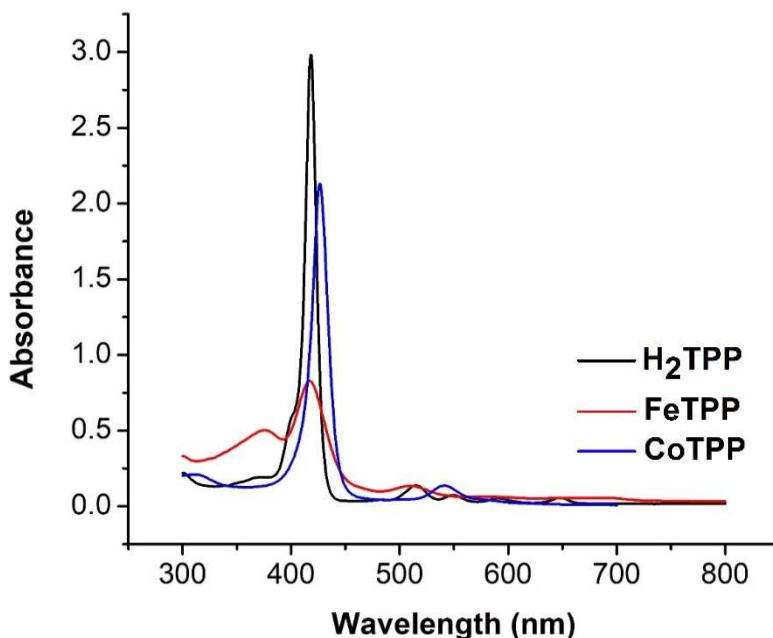


**Figure 3:** UV-visible absorbance spectrum of the clickable porphyrin without metal (black line), the clickable Fe porphyrin (red line), and the clickable Co porphyrin (blue line) in dichloromethane. The concentrations of the porphyrin were 310  $\mu$ M, 72  $\mu$ M, and 190  $\mu$ M, respectively.

### 2.2.5. Synthesis of 11-azidoundecan-1-ol

This compound was synthesized using a published procedure.[21] 11-bromo-1-undecanol (10.0 g, 39.8 mmol) and NaN<sub>3</sub> (3.0 g, 46.1 mmol) were dissolved in DMF (60 mL). The reaction was stirred at room temperature for 24 h and then quenched with H<sub>2</sub>O (50 mL). After extraction with CHCl<sub>3</sub> (30 mL x3), washing with water (30 mL x3), drying via anhydrous Na<sub>2</sub>SO<sub>4</sub>, removing the solvent *in vacuo* and setting in an oven overnight at ~100°C, 11-azidoundecan-1-ol (8.5 g, 100% yield) was obtained as a yellow viscous oil. <sup>1</sup>H NMR (400 MHz in CDCl<sub>3</sub>) δ 3.63 (t, 2H, J = 6.6 Hz), 3.25 (t, 2H, J = 6.6 Hz), 1.25-1.64 (m, 18H).

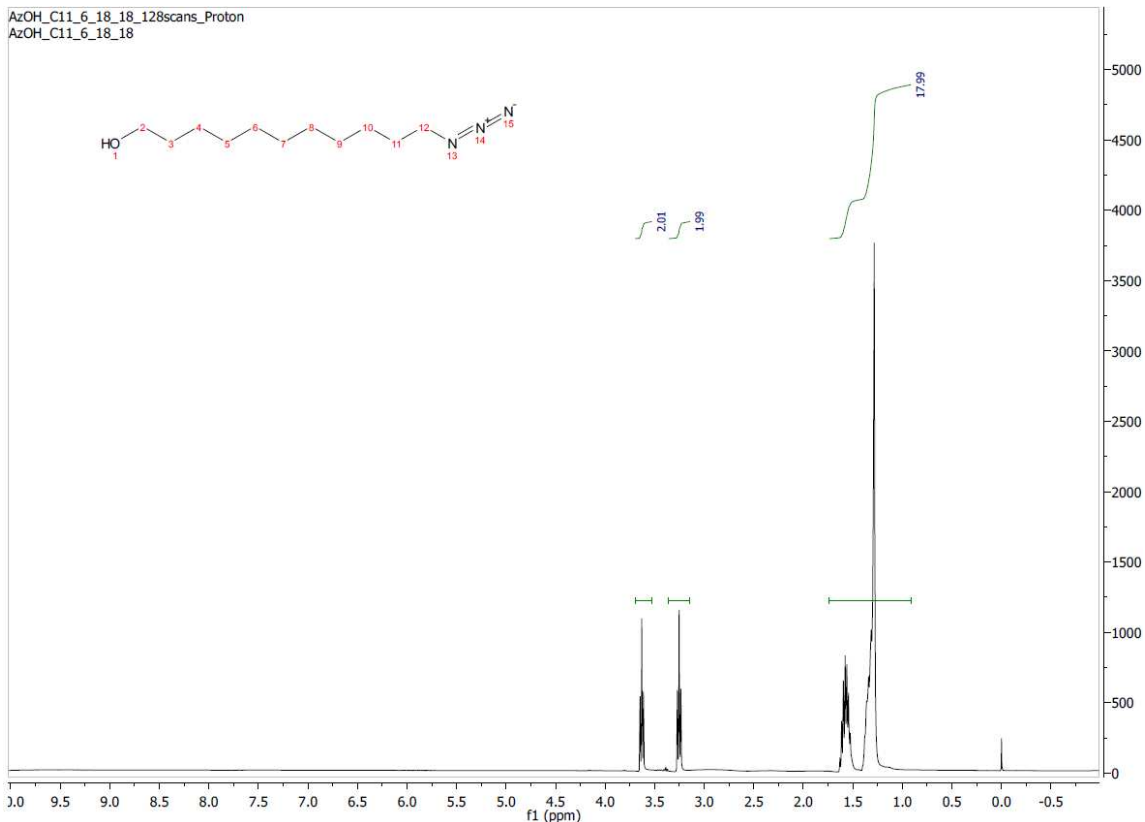


**Figure 4:** <sup>1</sup>H NMR spectrum of 11-azido-1-undecanol.

### 2.2.6. Synthesis of 11-azidoundecyldihydrogen phosphate

11-azidoundecan-1-ol (4.2 g, 20 mmol) and trimethylamine (3.11 mL, 22 mmol) were stirred together in anhydrous THF in an ice bath. POCl<sub>3</sub> (2.07 mL, 22 mmol) was immediately added into the solution dropwise. The resulting solution was stirred for 5 h and quenched with H<sub>2</sub>O. The crude product was extracted with CHCl<sub>3</sub> (30 mL, 3x), washed with water (30 mL, 3x), and dried with anhydrous Na<sub>2</sub>SO<sub>4</sub>. After removing the solvent *in vacuo* and further drying the product in an oven overnight at ~100°C, 11-azidoundecyl dihydrogen phosphate (4.9 g, 85% yield) was obtained as a viscous yellow oil. <sup>1</sup>H NMR (400 MHz in CDCl<sub>3</sub>) δ 10.63 (s, 2H), 4.03 (q, 2H, J = 6.7 Hz), 3.25 (t, 2H, J = 7.0 Hz), 1.25-1.72 (m, 18H).

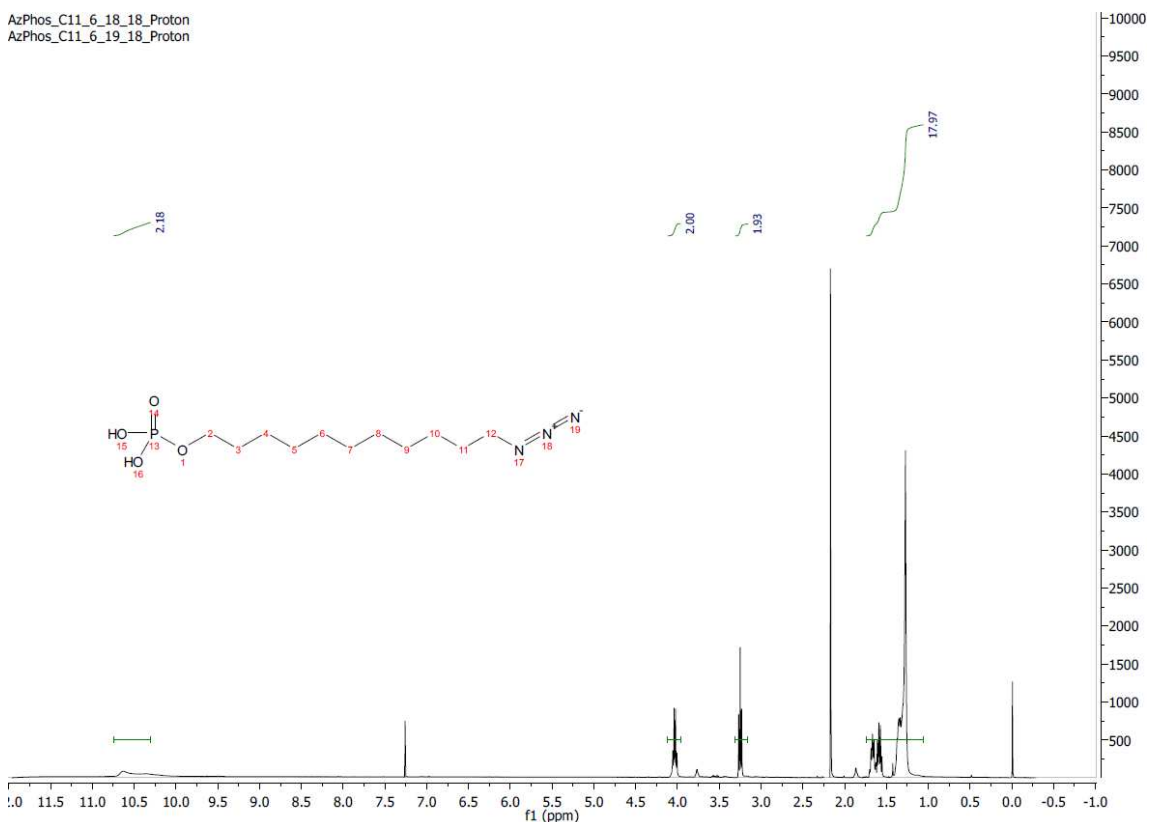


**Figure 5:** <sup>1</sup>H NMR spectrum of 11-azidoundecylphosphonic acid. The singlet at 2.17 ppm is due to residual acetone.

### *2.2.7. Synthesis of 5-azidopentan-1-ol and 16-azidohexadecan-1-ol*

These syntheses followed the same procedures as the 11-azidoundecan-1-ol analogue above starting with 5-bromo-1-pentanol (5 mL, 41.3 mmol) and 16-bromo-1-hexadecanol (0.5 g, 1.56 mmol), respectively. 5-azidopentan-1-ol (4.4 g, 72% yield) was obtained as a non-viscous yellow liquid while 16-azidohexadecan-1-ol (0.42 g, 95.26% yield) was obtained as a white solid.

### *2.2.8. Synthesis of 5-azidopentyldihydrogen phosphate and 16-azidohexadecyldihydrogen phosphate*

These syntheses followed the same procedures as the 11-azidoundecyldihydrogen phosphate analogue above using 5-azidopentan-1-ol (2.58 g, 20 mmol) and 16-azidohexadecan-1-ol (0.42 g, 1.48 mmol), respectively. 5-azidopentyldihydrogen phosphate (1.43 g, 32% yield) was obtained as a clear yellow tinted liquid while 16-azidohexadecyldihydrogen phosphate (0.52 g, 97% yield) was obtained as a white solid.

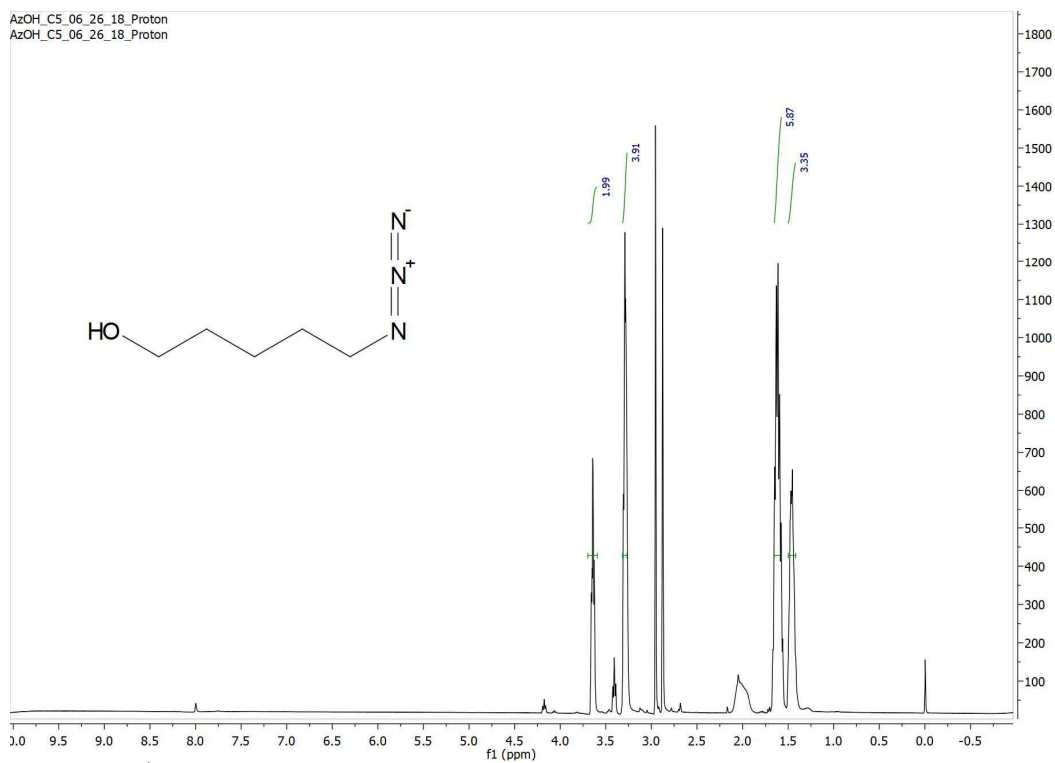


Figure 6: <sup>1</sup>H NMR spectrum of 5-azido-1-pentanol.

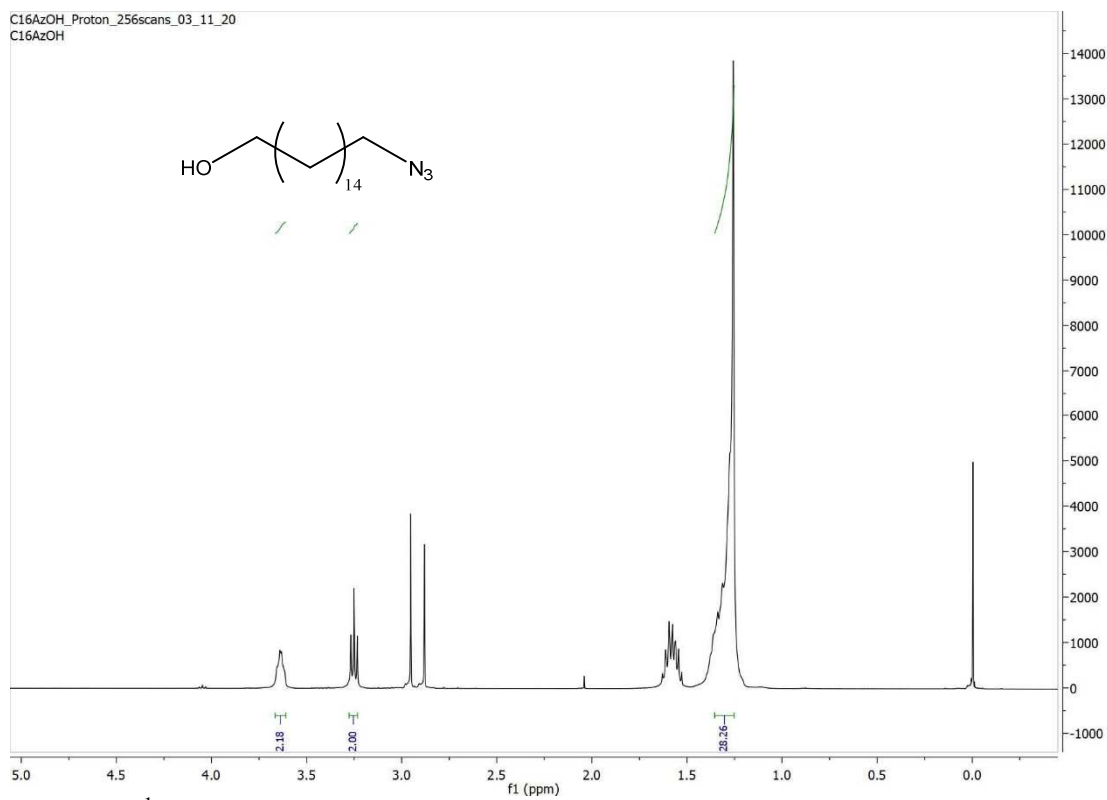
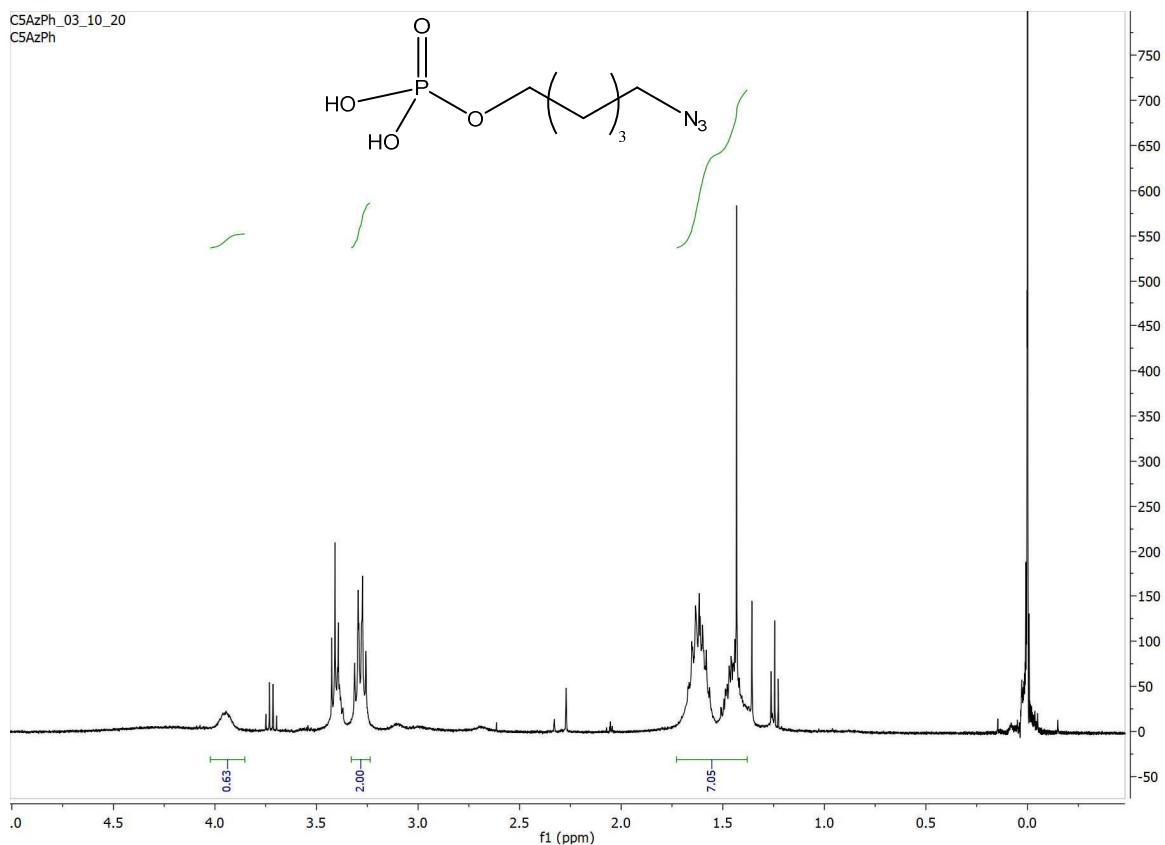


Figure 7: <sup>1</sup>H NMR spectrum of 16-azido-1-hexadecanol.



**Figure 8:** <sup>1</sup>H NMR spectrum of 5-azidopentyl dihydrogen phosphate.

### 2.3. Experiments with Au Electrodes

Au electrodes had an immersed geometric surface area of 0.218 cm<sup>2</sup>. A thiol solution in ethanol containing 1-azido-11-undecanethiol (100 μM) with LiClO<sub>4</sub> (100 mM) was added to the Au electrodes. The self-assembled monolayers (SAMs) were formed electrochemically by cycling between 0 V and -0.7 V four times at a scan rate of 10 mV/s. Similar electrochemical procedures have been used to form thiol-based SAMs previously.[22] The Au electrodes were subsequently rinsed three times with ethanol and de-ionized water. The azide-alkyne click solution was prepared by combining 2.3 mL 3:1 vol % DMSO and water, 300 μL aqueous Cu(NO<sub>3</sub>)<sub>2</sub> (8 mM), 300 μL tris[(1-benzyl-1H-1,2,3-triazol-4-yl)methyl]amine (TBTA, 8 mM) in DMSO, 30 μL aqueous sodium

ascorbate (100 mM), and 72  $\mu\text{L}$  FeTPP (4 mM) in DMSO. About 300  $\mu\text{L}$  of the click solution was added on each surface and allowed to sit on the surfaces for 1 hour in the dark. The Au electrodes were then rinsed three times with water before linear sweep voltammetry (LSV) was performed. pH 7 buffer solutions were sparged with  $\text{O}_2$  or  $\text{N}_2$  for 15 minutes prior to running each LSV experiment.

#### *2.4. Experiments with ITO and FTO Electrodes*

A solution of 5-azidopentyldihydrogen phosphate, 11-azidoundecyldihydrogen phosphate or 16-azidohexadecyldihydrogen phosphate in chloroform (10 mM) was added to the ITO or FTO electrodes and allowed to sit on the electrodes for 48 hr to generate the azide-terminated SAMs. The ITO and FTO electrodes were then rinsed successively with DCM, ethanol, and water. The azide-alkyne click solution was prepared by combining 2.3 mL 3:1 vol % DMSO and water, 300  $\mu\text{L}$  aqueous  $\text{Cu}(\text{NO}_3)_2$  (8 mM), 300  $\mu\text{L}$  tris[(1-benzyl-1H-1,2,3-triazol-4-yl)methyl]amine (TBTA, 8 mM) in DMSO, 300  $\mu\text{L}$  aqueous sodium ascorbate (100 mM), and 72  $\mu\text{L}$  FeTPP or CoTPP or  $\text{H}_2\text{TPP}$  (4 mM) in DMSO. For cyclic voltammetry (CV) experiments, the immersed geometric surface area of the ITO electrodes was 0.218  $\text{cm}^2$ . About 300  $\mu\text{L}$  of the click solution was added on each surface and allowed to sit on the surfaces for 1 hour in the dark. The ITO electrodes were then rinsed three times with water. CVs were conducted in aqueous  $\text{NaHCO}_3$  solutions (100 mM) that were sparged with  $\text{CO}_2$  or  $\text{N}_2$  for 15 minutes prior to running the electrochemistry. Linear sweep voltammograms are presented as an average of 3-4 individual trials.

##### *2.4.1 Surface Coverage Calculations*

The calculated surface coverage of  $1.3 \times 10^{15}$  molecules/ $\text{cm}^2$  originates from integrating the average amount of charge under the  $\text{Fe}^{2+}/\text{Fe}^{3+}$  couple. This calculation

assumes a flat ITO surface. From AFM, the average roughness of the ITO is determined to be 3.6, which when taken into account decreases the surface coverage for a theoretically perfectly flat ITO substrate to  $3.6 \times 10^{14}$  molecules/cm<sup>2</sup>. The adsorption cross section of cobalt(II) 5,10,15,20-tetraphenylporphyrin has experimentally been determined to be 1.41 nm by 1.41 nm when lying flat on an electrode.[23] Due to the long-chained alkyl phosphate linkers present in our system, the porphyrins cannot lie flat and instead likely stack vertically to maximize  $\pi$ - $\pi$  interactions. Using Spartan '08 (Wavefunction, Inc.) v. 1.2.0, the intermolecular spacing of FeTPP with bound water ligands is modeled to be 0.71 nm, giving an effective area on the electrode of 1.41 nm by 0.71 nm for each molecule. Assuming a perfectly packed monolayer, this value gives a theoretical surface coverage of  $1.0 \times 10^{15}$  molecules/cm<sup>2</sup> for a flat ITO surface, which is close to the experimentally-derived value (~2.8 times higher). This overestimation is expected since AFM images show a less-than-ideally packed monolayer of porphyrin on the electrode.

### *2.5. Quantification of Formate Production using <sup>1</sup>H NMR Spectroscopy*

The immersed geometric surface area of ITO and FTO electrodes for formate detection was 20 cm<sup>2</sup>, and the volume of click solution used was increased to 21 mL. Chronoamperometry was performed in CO<sub>2</sub>-sparged aqueous NaHCO<sub>3</sub> (100 mM) for 1 hour at -1.6 V, -1.4 V and -1.2 V. Afterwards, the solution was transferred to a round bottom flask and removed under reduced pressure. D<sub>2</sub>O (1 mL) was used to dissolve the residual salts, and 10  $\mu$ L acetic acid was added as an internal standard. The formate peak at 8.5 ppm was used for product quantification.

### *2.6. Quantification of Gaseous Products using Gas Chromatography*

The immersed geometric surface area of ITO and FTO electrodes for gaseous product detection was 5.1 cm<sup>2</sup>, and the volume of click solution used was 2.5 mL. Chronoamperometry at -1.6 V, -1.4 V and -1.2V for 1 hour was carried out using a modified custom-built electrochemical cell equipped with gas-tight valves. The headspace of the cell was 10.9 mL. After chronoamperometry, 20 mL of air from a syringe was used to push the gaseous product out of the cell into a gas chromatograph (SRI 8610C MG#5). A four-part profile was used to modulate the temperature of the columns. The columns were held at 50°C for 1 minute before ramping the temperature to 90°C over the course of 2 minutes. Next, the columns were held at 90°C for 3 minutes before ramping the temperature to 270°C over the course of 6 minutes. CO in N<sub>2</sub> (Cal Gas Direct, Inc.) was used as a standard and elutes at 4.3 minutes using this profile. CO from the catalysts was detected at the same elution time as the standard. No methane, ethane, or ethylene was detected.

### *2.7. Atomic Force Microscopy*

Atomic force microscopy (AFM) images were obtained using a Nanosurf EasyScan 2 microscope operated in contact mode using a silicon tip with an aluminum reflective coating (ContAl-G, TedPella, Inc.).

## **3. Results and discussion**

### *3.1. Porphyrin Electrocatalysts on Au Electrodes for O<sub>2</sub> Reduction*

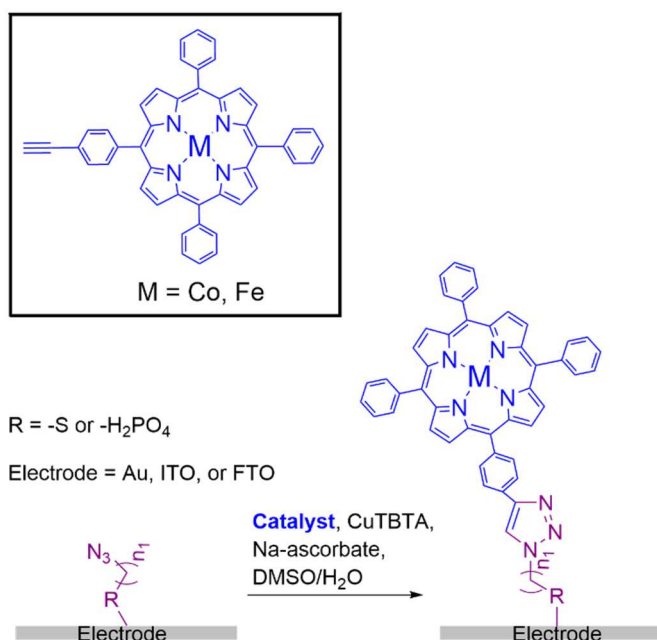
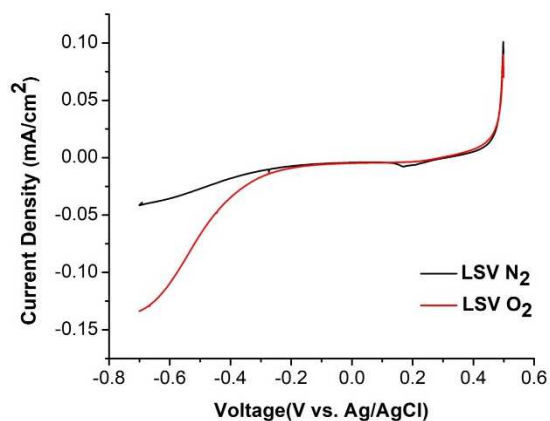


**Figure 9:** Schematic of the attachment of porphyrin catalysts to Au or ITO electrodes using azide-alkyne click chemistry.

We first synthesized alkyne-modified Fe and Co tetraphenylporphyrins (FeTPP and CoTPP) so that they could be attached via azide-alkyne click chemistry on azide-modified working electrodes. We then attached the catalysts to azide-terminated SAMs on Au electrodes formed with 1-azido-11-undecanethiol. We evaluated the

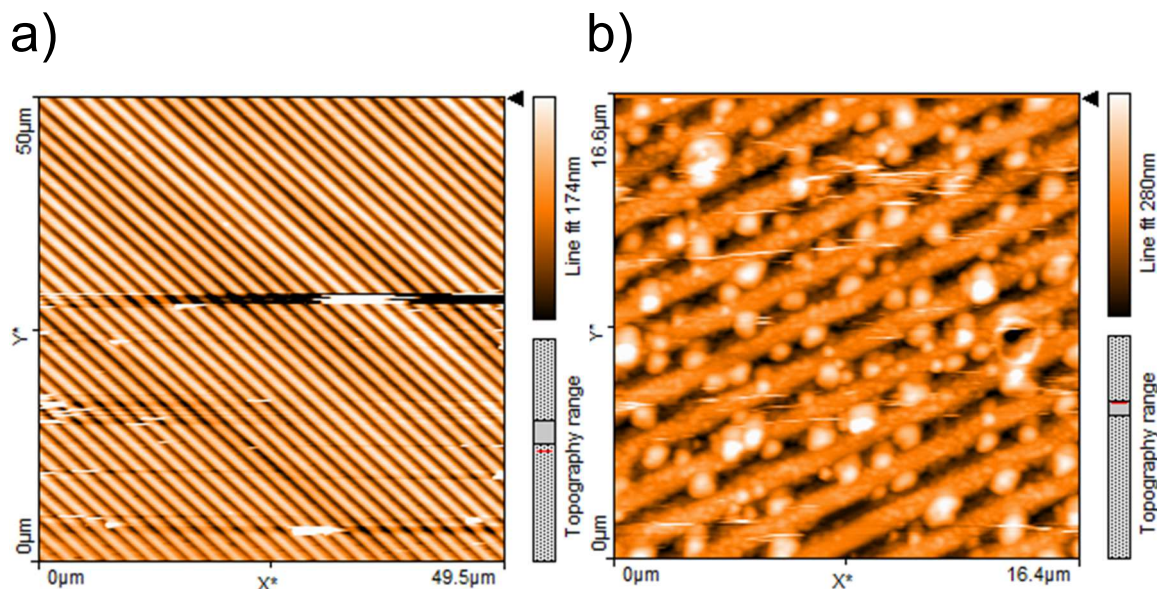
ability of the catalysts to electrochemically reduce O<sub>2</sub> since SAMs of Fe porphyrins on Au electrodes are well known to catalyze the O<sub>2</sub> reduction reaction.[24]

Figure 10 compares linear sweep voltammograms (LSVs) of a SAM of FeTPP in pH 7 buffer sparged with N<sub>2</sub> or O<sub>2</sub>. The cathodic catalytic current of FeTPP is significantly greater in the presence of O<sub>2</sub> as compared to N<sub>2</sub>, demonstrating that FeTPP was successfully attached to the Au electrode and that FeTPP is an active O<sub>2</sub> reduction catalyst as has been shown previously for similar Fe porphyrins.[25]



**Figure 10:** Linear sweep voltammograms of FeTPP-modified Au electrodes at 10 mV/s in a pH 7 phosphate buffer sparged with N<sub>2</sub> (black line) and O<sub>2</sub> (red line).

To further confirm that the porphyrin catalysts are attached to Au SAMs, we imaged unmodified and porphyrin-modified Au electrodes using atomic force microscopy (AFM, Figure 11). An AFM image of an unmodified Au electrode shows a uniformly spaced series of ridges  $\sim 2 \mu\text{m}$  in width (Figure 11A). Similar morphologies of Au electrodes using CD surfaces have been reported previously.[26] In contrast, an AFM image of a porphyrin-modified Au electrode shows spherical features embedded within and on the ridges (Figure 11B). We attribute these features to aggregates of porphyrin molecules since they are not present on unmodified Au surfaces (Figure 11A).



**Figure 11:** AFM images of unmodified Au (a) and CoTPP-modified Au (b) surfaces.

### 3.2. Porphyrin SAMs on ITO Electrodes

With the O<sub>2</sub> reduction catalytic activity of porphyrin SAMs verified on Au electrodes, we next evaluated the ability of SAMs of Fe and Co porphyrins to electrocatalytically reduce CO<sub>2</sub>. However, thiol-based SAMs on Au electrodes are not suitable because the thiol moiety is known to decompose at the highly reducing voltages needed for CO<sub>2</sub> reduction.[27] Therefore, we fabricated SAMs using 11-azidoundecyldihydrogen phosphate on ITO on glass electrodes since alkyl phosphates are known to both bind on ITO surfaces and be more electrochemically stable under reducing conditions.[28] After forming the azide-phosphate-modified ITO surfaces, we used azide-alkyne click chemistry to attach alkyne-modified porphyrins on the electrodes.

To verify the success of the click reaction, we performed an array of electrochemical and imaging experiments. First, we conducted cyclic voltammograms (CVs) of four different ITO electrodes in various states of surface modification (Figure 12). CVs of unmodified and SAM-modified ITO electrodes do not display any significant

cathodic or anodic redox peaks (Figures 12, black and red lines). However, the capacitance of the unmodified ITO electrode decreases from  $\sim 80 \mu\text{F}/\text{cm}^2$  to  $\sim 20 \mu\text{F}/\text{cm}^2$  upon formation of the phosphate SAM. This decrease in capacitance is expected because the distance between the electrochemical double layer and the ITO surface increases upon SAM formation. CVs of porphyrin without metal ( $\text{H}_2\text{TPP}$ ) and of  $\text{FeTPP}$  show clear cathodic and anodic redox peaks, the former due to redox associated with the porphyrin ring as described in pervious literature[29-31] and the latter due to the redox of  $\text{Fe}^{2+}/\text{Fe}^{3+}$  (Figures 12, blue and green lines). By integrating the charge under the  $\text{Fe}^{2+}/\text{Fe}^{3+}$  wave, we calculated that the amount of  $\text{FeTPP}$  catalyst attached to the surface is  $1.3 \times 10^{15}$  molecules/ $\text{cm}^2$ , a value that is similar to what is expected for a porphyrin monolayer on ITO.

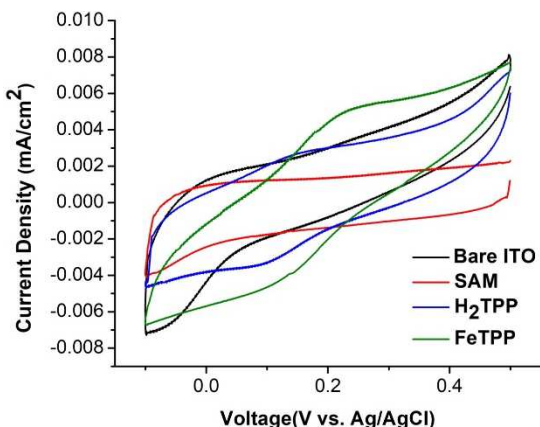


**Figure 12:** Cyclic voltammograms of unmodified ITO (black line) and ITO surfaces modified with SAM (red line),  $\text{H}_2\text{TPP}$  (blue line), and  $\text{FeTPP}$  (green line) at  $100 \text{ mV/s}$  in  $\text{CO}_2$ -sparged  $100 \text{ mM NaHCO}_3$ .

Another series of CV experiments was conducted using a potassium ferricyanide ( $\text{K}_3\text{Fe}(\text{CN})_6$ ) blocking test to assess attachment of porphyrin to the working electrode. A CV of an unmodified ITO working electrode in  $\text{K}_3\text{Fe}(\text{CN})_6$  yields a reversible redox wave with peak current densities of  $\sim 0.1 \text{ mA}/\text{cm}^2$  (Figure 13, black line). The unmodified ITO electrode allows for free diffusion of  $\text{Fe}(\text{CN})_6^{3-}$  to the surface of the working electrode,

giving rise to the reversible wave. Upon attaching a SAM of 11-azidoundecyldihydrogen phosphate to the ITO surface, the diffusion of  $\text{Fe}(\text{CN})_6^{3-}$  is hindered by the SAM, thus decreasing the cathodic and anodic current density (Figure 13, red line). The peak-to-peak separation of the redox couple also increases, which indicates that the kinetics of the reaction are impeded by the SAM. Upon attachment of porphyrin and increasing length of the monolayer, diffusion of free  $\text{Fe}(\text{CN})_6^{3-}$  from solution to the ITO surface is dramatically reduced. This decrease is evidenced by almost a complete disappearance of the cathodic and anodic peaks when either  $\text{H}_2\text{TPP}$  or  $\text{FeTPP}$  is clicked onto the monolayer (Figure 13, blue and green lines).

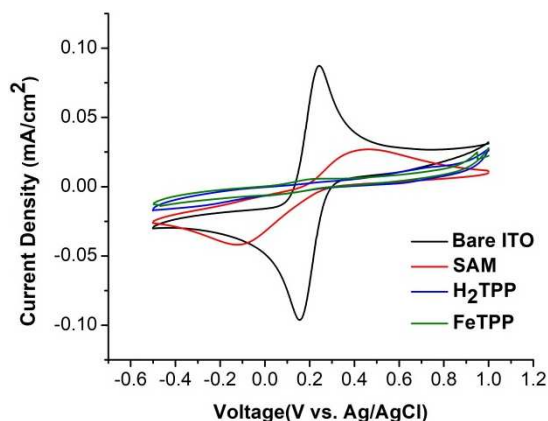


**Figure 13:** Cyclic voltammograms of unmodified ITO (black line) and ITO surfaces modified with SAM (red line),  $\text{H}_2\text{TPP}$  (blue line), and  $\text{FeTPP}$  (green line) at 50 mV/s in 1 mM  $\text{K}_3\text{Fe}(\text{CN})_6$  with 100 mM NaCl in  $\text{H}_2\text{O}$ .

We recorded AFM images comparing unmodified ITO surfaces and ITO modified with  $\text{CoTPP}$ . For unmodified ITO surfaces, the clear, granular network reported previously [32, 33] is evident (Figures 14a and 14b). With  $\text{CoTPP}$  attached to the ITO (Figures 14c and 14d), the granular pattern is diminished and replaced by spherical features similar to the features on the porphyrin-modified gold (Figure 11b). These AFM images, in conjunction with the previously described electrochemical experiments, validate the

success of the azide-alkyne click reaction and attachment of porphyrin catalyst to the ITO working electrode surface.

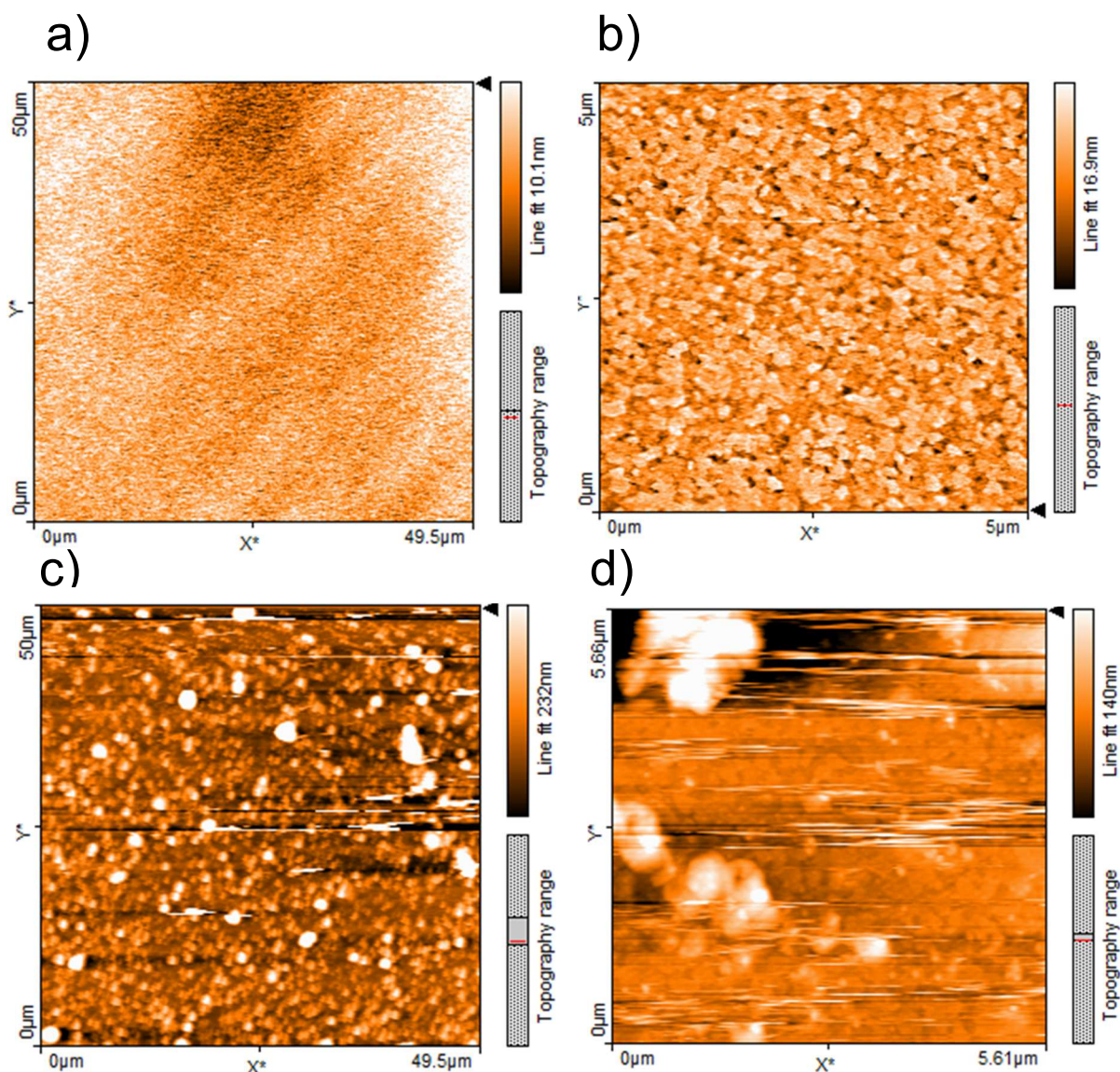


**Figure 14:** AFM images of unmodified ITO (a, b) and CoTPP-modified ITO (c, d) surfaces.

### 3.3. Electrocatalytic $\text{CO}_2$ Reduction using Porphyrin ITO SAMs

To assess the ability of SAMs of porphyrins to catalyze the reduction of  $\text{CO}_2$ , CVs were conducted in bicarbonate solutions sparged with  $\text{CO}_2$  or  $\text{N}_2$ . CVs of a SAM of FeTPP

exhibit greater cathodic current density in N<sub>2</sub>-sparged solution as compared to the solution containing CO<sub>2</sub> (Figure 15a). The greater current density under N<sub>2</sub> demonstrates that the FeTPP SAM catalyzes H<sub>2</sub> evolution from the reduction of H<sub>2</sub>O and at first glance suggests that the SAM is inactive towards CO<sub>2</sub>. However, experiments with Cu metal, a well-known CO<sub>2</sub> catalyst [34] exhibit similar behavior wherein CVs in N<sub>2</sub>-sparged buffer yield more current than in CO<sub>2</sub>-sparged solutions (Figure 16). The lower current for the CVs with CO<sub>2</sub> are due to CO<sub>2</sub> binding the metals in the catalysts, thus partially blocking protons from binding the metals, which results in reduced overall catalytic current. In other words, in CO<sub>2</sub>-sparged solution, there is a competition between CO<sub>2</sub> and protons binding to metal active sites. This competition is absent in N<sub>2</sub>-sparged solution, which results in greater H<sub>2</sub> evolution. A CoTPP-modified surface was also studied in both CO<sub>2</sub>-sparged and N<sub>2</sub>-sparged solutions (Figure 15b). Contrary to the FeTPP surface, the current density remains similar for both sparged solutions, and the overpotential in CO<sub>2</sub>-sparged solution decreases compared to the CV in N<sub>2</sub>-sparged solution. This lower overpotential implies a lower energy barrier for product evolution and is direct evidence that CO<sub>2</sub> reduction occurs. CV experiments using unmodified ITO, SAM-modified ITO, and H<sub>2</sub>TPP-modified ITO exhibit subtle shifts in current densities and overpotentials that further suggest the FeTPP and CoTPP catalysts are attached to the SAMs (Figure 17).

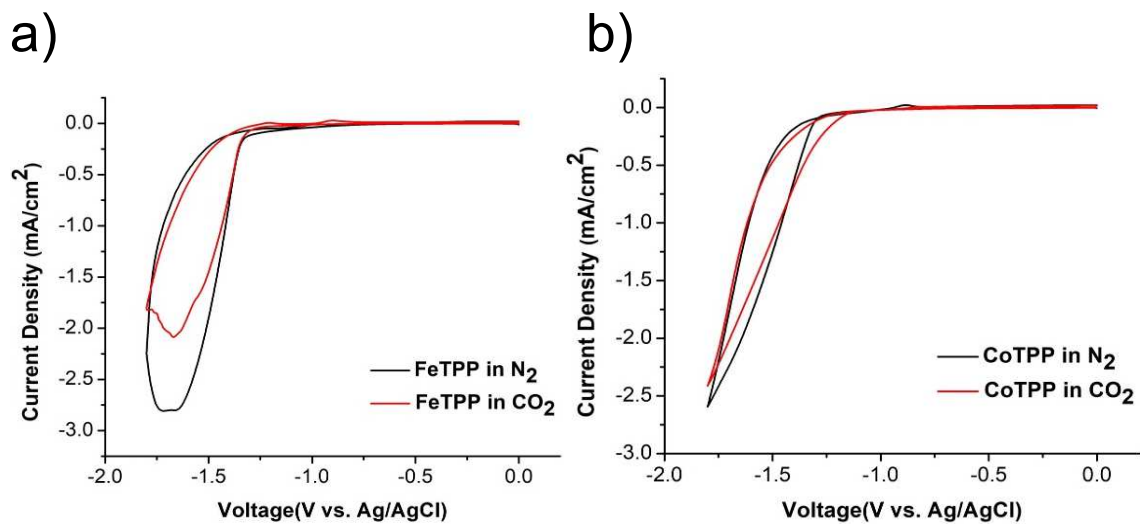


**Figure 15:** Cyclic voltammograms of ITO electrodes modified with FeTPP (a) and CoTPP (b) in 100 mM NaHCO<sub>3</sub> sparged with N<sub>2</sub> (black lines) and CO<sub>2</sub> (red lines) at 10 mV/s.

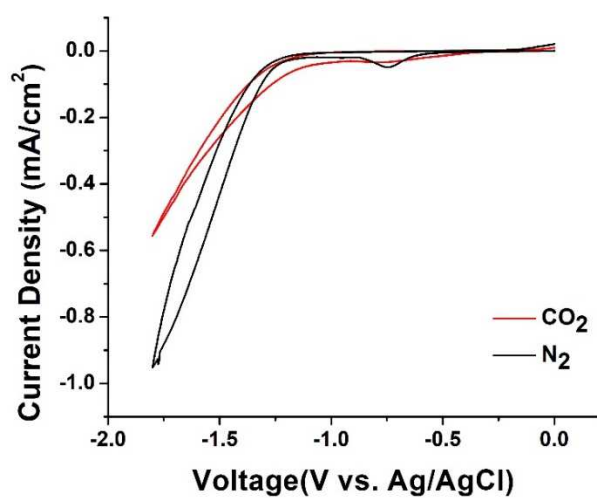


**Figure 16:** Cyclic voltammograms of Cu foil in 100 mM NaHCO<sub>3</sub> sparged with CO<sub>2</sub> (red line) and N<sub>2</sub> (black line) at 10 mV/s.

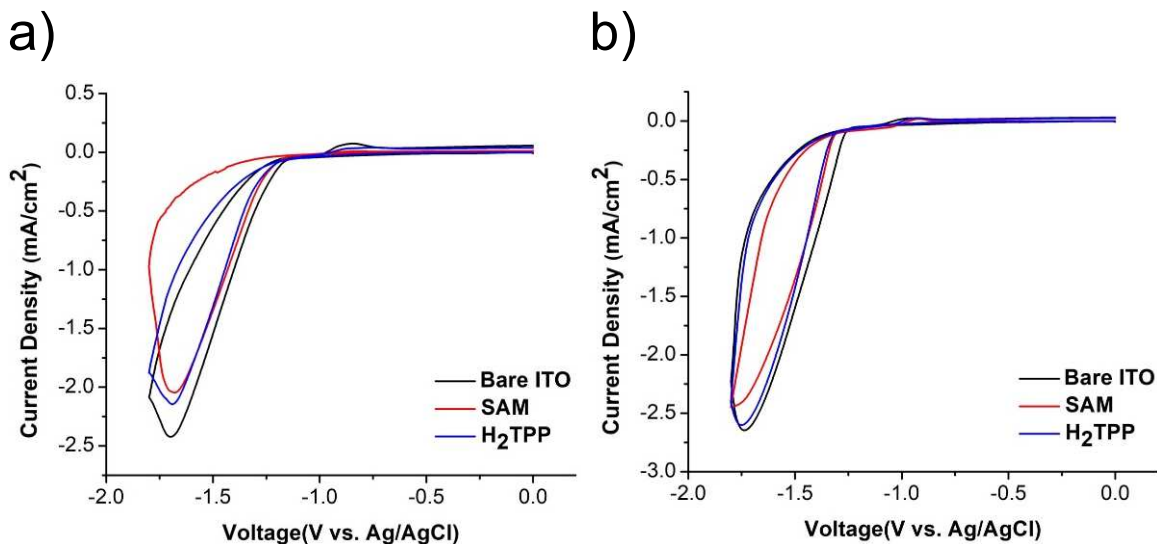


**Figure 17:** Cyclic voltammograms of unmodified ITO (black lines) and ITO modified with SAM (red lines) and H<sub>2</sub>TPP (blue lines) in 100 mM NaHCO<sub>3</sub> sparged with CO<sub>2</sub> (a) and N<sub>2</sub> (b) at 10 mV/s.

Chronoamperometry was carried out at -1.6V for 1 hour to determine products formed during CO<sub>2</sub> reduction conditions. Unmodified ITO (Figure 18a, black line) shows a quick decline in cathodic current throughout the duration of time, with a total of 2.1 C of charge generated. Surfaces modified with CoTPP (Figure 18a, blue line) show a decrease in current density and stabilization around -0.1 mA/cm<sup>2</sup> resulting in 5.5 C. The increased steady-state cathodic current density and charge passed of the porphyrin altered surface demonstrate that the catalyst is more active than unmodified ITO throughout the time course of the experiment.

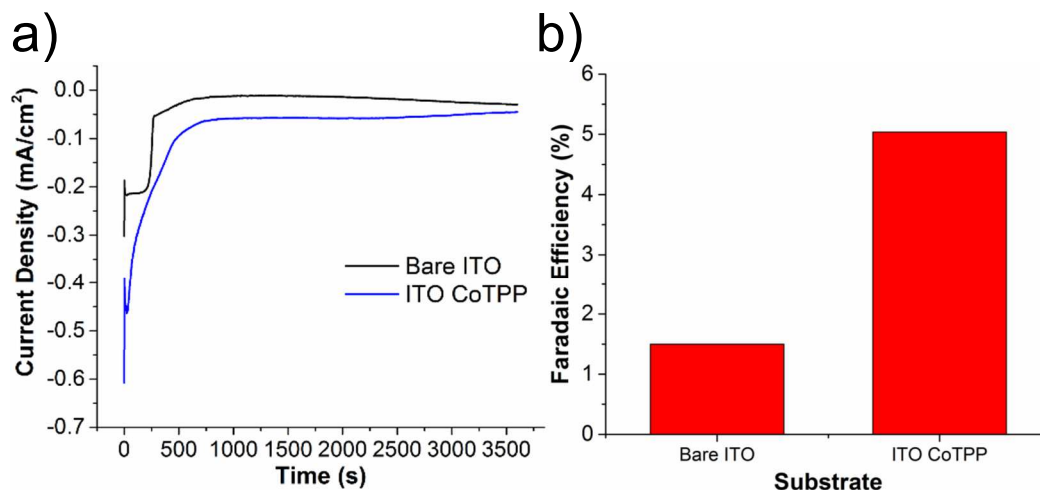


**Figure 18:** Chronoamperometry at -1.6 V of unmodified ITO (black line) and ITO modified with CoTPP (blue line) in 100 mM NaHCO<sub>3</sub> sparged with CO<sub>2</sub> (a) and faradaic efficiencies for each surface (b).

From chronoamperometry experiments, the gaseous samples were injected into a gas chromatography instrument to analyze product formation. While no methane, ethylene,

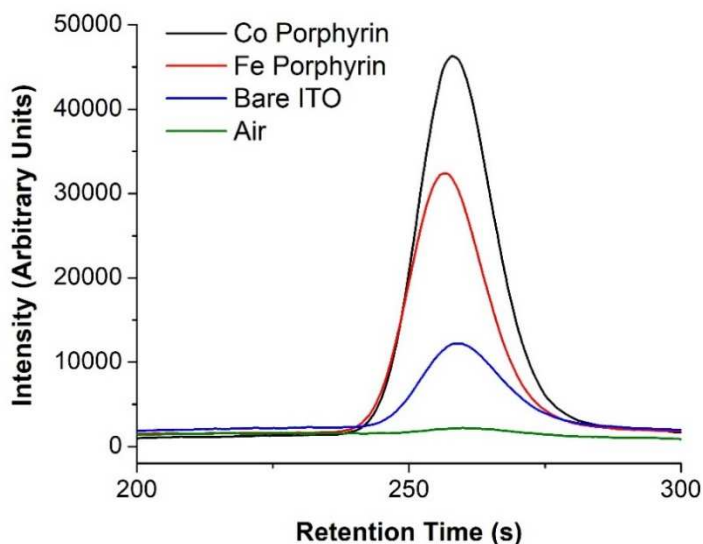


**Figure 19:** Gas chromatograms of the CO peak formed after chronoamperometry at -1.6 V for 1 hour using an unmodified ITO electrode (blue line) and ITO modified with CoTPP (black line) and FeTPP (red line). The green line represents an air sample.

or ethane were detected, carbon monoxide was detected in all unmodified and modified surfaces as shown in Figure 19. Integration of the CO peaks in each chromatogram allowed for calculation of each Faradaic efficiency and resulted in the bar graph shown in Figure 18b. The resulting faradaic efficiencies of unmodified ITO

and CoTPP modified ITO are 1.5% and 5.04%, respectively. These meager yields warranted an investigation into substrate performance and CO<sub>2</sub> sparging parameters.

### 3.4 Effects of Substrate on Electrocatalytic CO<sub>2</sub> Reduction

The components of ITO, tin-doped indium oxide, are easily reduced at CO<sub>2</sub> reduction potentials. Indium is reduced at various reduction potentials vs. SHE for several oxidation states (figure 20a.) Tin is also shown to be reduced at various potentials at several oxidation states within our potential window (figure 20b.)

In <sup>+</sup> + e ⇌ In	-0.14	Sn <sup>2+</sup> + 2 e ⇌ Sn	-0.1375
In <sup>2+</sup> + e ⇌ In <sup>+</sup>	-0.40	Sn <sup>4+</sup> + 2 e ⇌ Sn <sup>2+</sup>	0.151
In <sup>3+</sup> + e ⇌ In <sup>2+</sup>	-0.49	Sn(OH) <sub>3</sub> <sup>+</sup> + 3 H <sup>+</sup> + 2 e ⇌ Sn <sup>2+</sup> + 3 H <sub>2</sub> O	0.142
In <sup>3+</sup> + 2 e ⇌ In <sup>+</sup>	-0.443	SnO <sub>2</sub> + 4 H <sup>+</sup> + 2 e ⇌ Sn <sup>2+</sup> + 2 H <sub>2</sub> O	-0.094
In <sup>3+</sup> + 3 e ⇌ In	-0.3382	SnO <sub>2</sub> + 4 H <sup>+</sup> + 4 e ⇌ Sn + 2 H <sub>2</sub> O	-0.117
In(OH) <sub>3</sub> + 3 e ⇌ In + 3 OH <sup>-</sup>	-0.99	SnO <sub>2</sub> + 3 H <sup>+</sup> + 2 e ⇌ SnOH <sup>+</sup> + H <sub>2</sub> O	-0.194
In(OH) <sub>4</sub> <sup>-</sup> + 3 e ⇌ In + 4 OH <sup>-</sup>	-1.007	SnO <sub>2</sub> + 2 H <sub>2</sub> O + 4 e ⇌ Sn + 4 OH <sup>-</sup>	-0.945
In <sub>2</sub> O <sub>3</sub> + 3 H <sub>2</sub> O + 6 e ⇌ 2 In + 6 OH <sup>-</sup>	-1.034	H <sub>2</sub> SnO <sub>3</sub> <sup>-</sup> + H <sub>2</sub> O + 2 e ⇌ Sn + 3 OH <sup>-</sup>	-0.909
		Sn(OH) <sub>6</sub> <sup>2-</sup> + 2 e ⇌ H <sub>2</sub> SnO <sub>3</sub> <sup>-</sup> + 3 OH <sup>-</sup> + H <sub>2</sub> O	-0.93
		Sr <sup>+</sup> + e ⇌ Sr	-4.10
		Sr <sup>2+</sup> + 2 e ⇌ Sr	-2.899
		Sr <sup>2+</sup> + 2 e ⇌ Sr(Hg)	-1.793
		Sr(OH) <sub>2</sub> + 2 e ⇌ Sr + 2 OH <sup>-</sup>	-2.88

**Figure 20:** Common reduction potentials for the components indium and tin in ITO substrate.[35]

The reduction potentials of indium and tin, along with the previous Faradaic efficiency results, show that the working electrode itself can be a hindrance to high catalytic reduction of CO<sub>2</sub> via substrate degradation. Fluorine-doped tin oxide however, FTO, only has one component that reduces within the electrochemical window. The current density under similar reduction conditions using FTO as a working electrode greatly increases as shown in Figure 21a. A greater current density compared to ITO could signify a greater capacity to propel electron transfer to the porphyrins without degrading the substrate. Further analysis of ITO degradation compared to FTO can be seen in Figure 21b wherein ITO and FTO surfaces were swept cathodically from 0 V and ending at four different

potentials (-1.8V, -1.6V, -1.4V, -1.2V). It is clear that the components of FTO are reduced to a far lesser degree at several voltages, possibly allowing for more stable porphyrin attachment and greater coalescence of charge. These results establish a premise to explore porphyrin altered FTO surfaces for electrocatalytic CO<sub>2</sub> reduction.

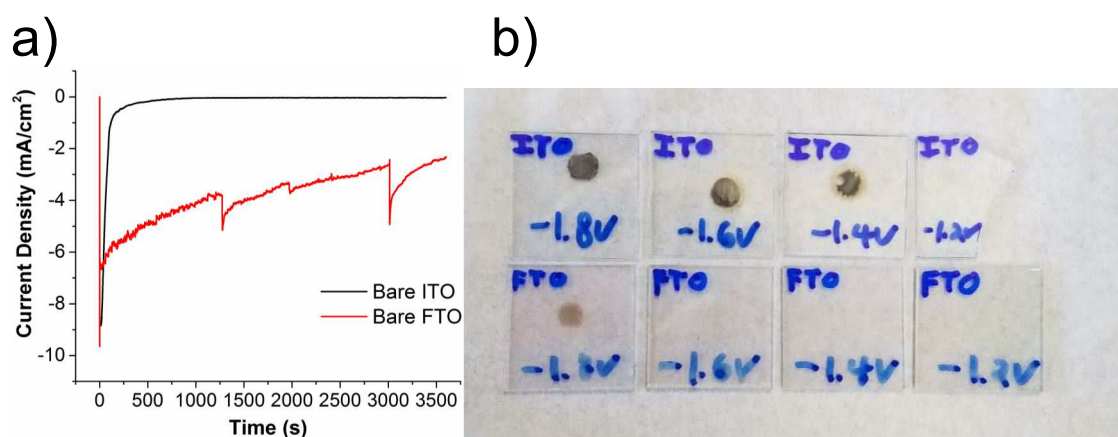
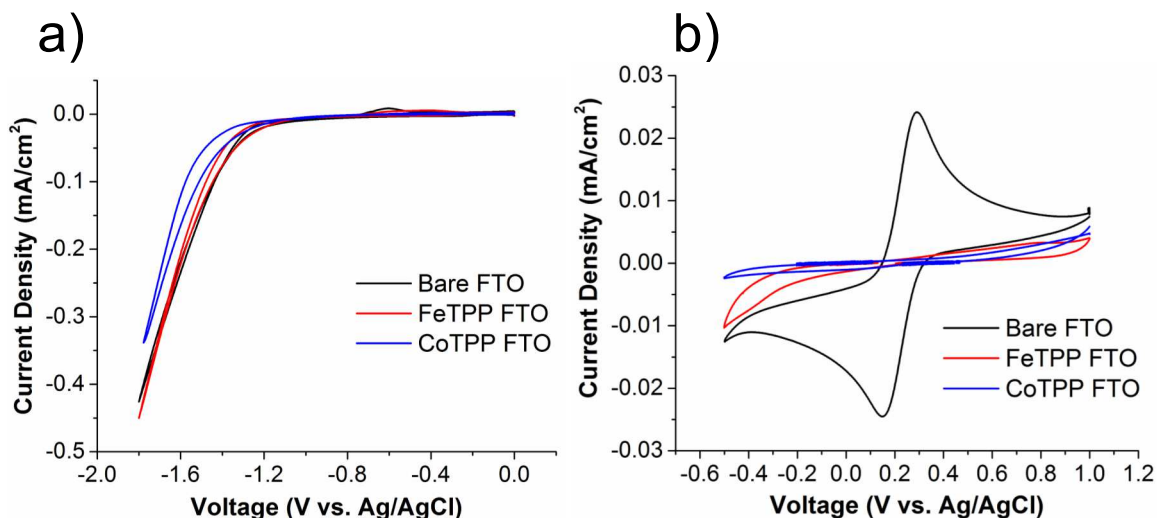


**Figure 21:** A comparison between the chronoamperometry of bare ITO and bare FTO at -1.6V in 100 mM NaHCO<sub>3</sub> sparged with CO<sub>2</sub> (a) and photographs of substrates after voltammetry experiments starting at 0 V sweeping to different negative voltages between ITO and FTO substrates (b).

### 3.5 Electrocatalytic CO<sub>2</sub> Reduction using Porphyrin FTO SAMs

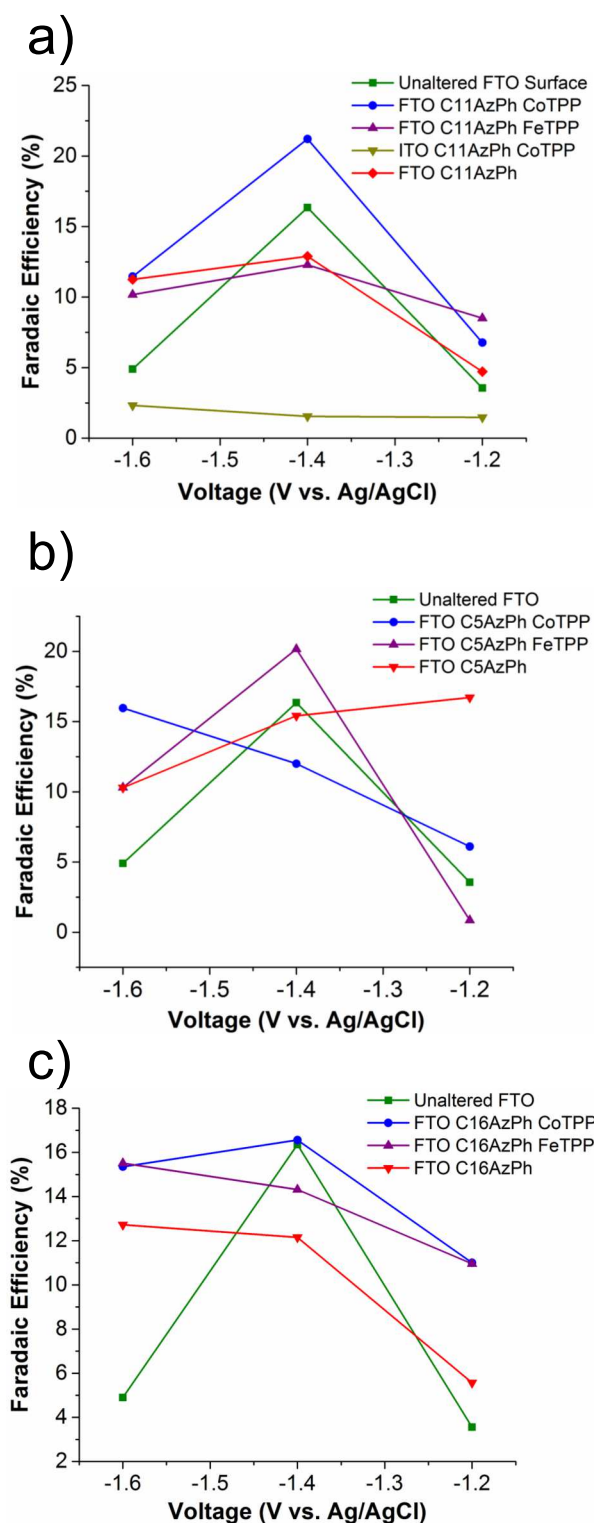
To compare the reduction properties of SAMs of porphyrins on FTO with that of ITO, CVs were conducted in bicarbonate solutions sparged with CO<sub>2</sub>. CVs of a SAM of CoTPP on FTO show less cathodic current density than that of bare FTO, but a higher overpotential. A FeTPP modified surface was also studied in similar electrochemical conditions producing similar current density and overpotential to the unmodified FTO surface (Figure 22a). Furthermore, a potassium ferricyanide blocking test was carried out on the unaltered and porphyrin altered surfaces to assess catalyst attachment (Figure 22b). Similar to the porphyrin altered surfaces on ITO, the current density greatly decreases for

FeTPP and CoTPP compared to unaltered FTO, showing that free  $\text{Fe}(\text{CN})_6^{3-}$  is being prevented from reaching the electrode surface as evidenced by porphyrin attachment.



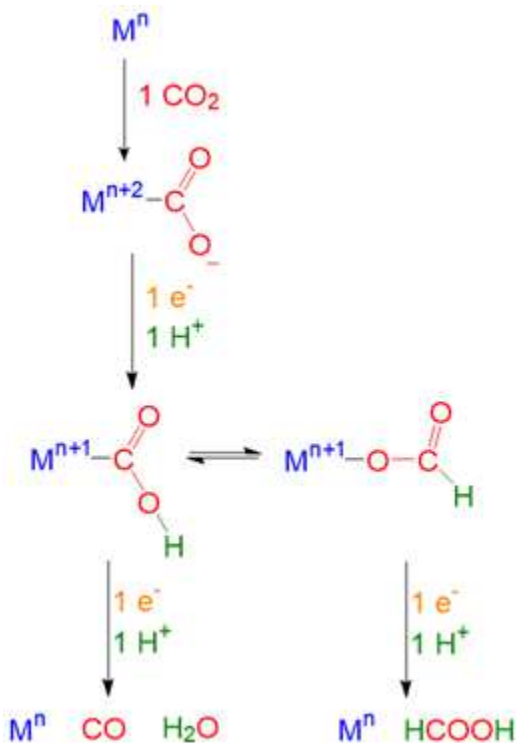
**Figure 22:** Cyclic voltammogram of FTO electrodes modified with FeTPP and CoTPP porphyrins in 100 mM  $\text{NaHCO}_3$  sparged with  $\text{CO}_2$  (a) and cyclic voltammogram (b) of unmodified FTO (black line) and FTO surfaces modified with FeTPP (red line) and CoTPP (blue line) at 50 mV/s in 1 mM  $\text{K}_3\text{Fe}(\text{CN})_6$  with 100 mM NaCl.

Chronoamperometry was carried out with continuous flow of  $\text{CO}_2$  at -1.6V, -1.4V and -1.2V for 1 hour to determine products formed during  $\text{CO}_2$  reduction conditions. Continuous flow of  $\text{CO}_2$  throughout the duration of the experiment was realized to be necessary for sufficient Faradaic efficiencies and analysis of reduction chemistry. Three different length azide-terminated phosphate SAMs of  $\text{C}_{11}$ ,  $\text{C}_5$  and  $\text{C}_{16}$  were studied at these three voltages to assess  $\text{CO}_2$  reduction properties towards CO production as shown in Figure 23. Such variance in SAM length allows insight into the role of electron transfer kinetics because longer-chained SAMs result in slower electron transfer dynamics than shorter-chained SAMs.[14] CoTPP modified  $\text{C}_{11}$  SAMs on ITO were also studied to compare Faradaic efficiencies between porphyrin modified electrodes of FTO and ITO (Figure 23a, yellow line).



**Figure 23:** Faradaic efficiencies at three voltages for C<sub>11</sub> SAM (a), C<sub>5</sub> SAM (b) and C<sub>16</sub> SAM (c).

It is clear that the Faradaic efficiencies of porphyrin modified ITO surface during constant low of CO<sub>2</sub> are miniscule to the Faradaic efficiencies of porphyrin modified FTO surfaces at all three voltages. Unmodified FTO surface (green line) shows heightened CO production at -1.4V, as do surfaces modified with only SAM (red line), FeTPP (purple line) and CoTPP (blue line.) From the C<sub>11</sub> SAM modified FTO surfaces, CoTPP has the highest Faradaic efficiency at -1.4 V at 21.2%. Experiments on C<sub>5</sub> SAM modified FTO surfaces (Figure 23b) also show a proclivity of CO production at -1.4 V. Here, FeTPP produces the highest Faradaic efficiency (purple line) at 20.2% compared to CoTPP (blue line.) C<sub>5</sub> azide-terminated SAMs allows for faster electron transport than C<sub>11</sub> azide-terminated SAMs.[14] One proposed mechanism of CO<sub>2</sub> reduction shown in



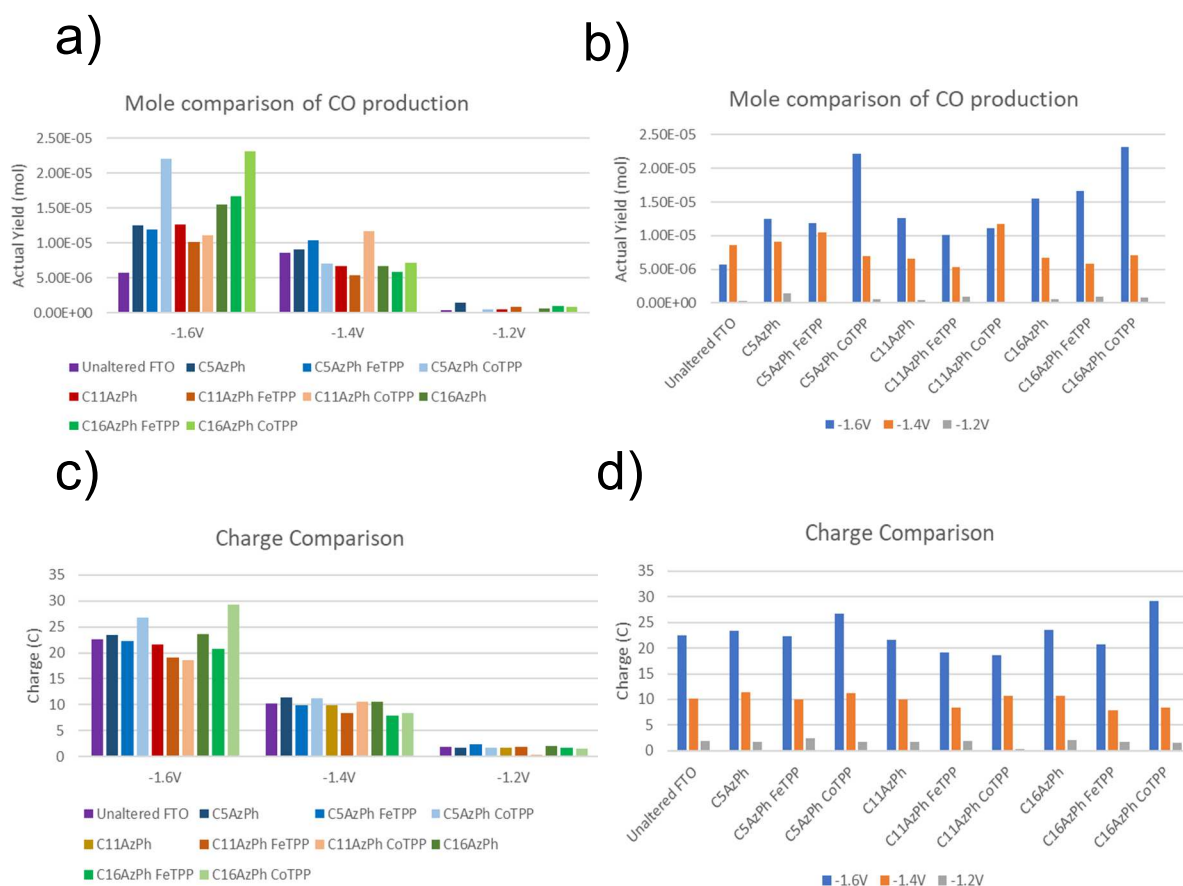
**Figure 24:** Proposed mechanism for electrocatalytic CO<sub>2</sub> reduction.

Figure 24 shows isomerization of the CO<sub>2</sub> molecule between carbon and oxygen attachment to the metal. Although both metals bond the carbon in CO<sub>2</sub> first, it has been reported that Fe is slightly more oxophilic than Co, typically favoring more formate production while Co favors CO production[36]. The counterintuitive results of C<sub>5</sub> SAM modified FeTPP surface at -1.4 V could be explained by proposing the fast electron kinetics reduce CO<sub>2</sub> before the molecule isomerizes, producing more CO than the CoTPP porphyrin.

Experiments on C<sub>16</sub> SAM modified FTO surfaces were also conducted with both porphyrins at all three voltages (Figure 23c). The preference of porphyrin to produce more CO at -1.4 V is still prevalent, and CoTPP generates higher faradaic efficiencies than FeTPP as was the case with C<sub>11</sub> SAM modified surfaces. Although the highest Faradaic efficiency is CoTPP at 16.56%, the Faradaic efficiencies between both porphyrins do not vary much. In fact, they are within 1% of each other at -1.2V and -1.6V. This could be since C<sub>16</sub> azide-terminated SAMs offer slow electron transfer kinetics [14], and this long of a chain length has ultimately rate limited electron migration. Although Faradaic efficiencies are the defining criteria for promising electrocatalysts, looking at other parameters of the reaction can be insightful as well. Figure 25 illustrates a complete picture of the actual number of moles CO produced along with charge passed for each experiment.

It is interesting to note the extreme amount of charge and moles of CO produced for the kinetically slow electron transfer rates of C<sub>16</sub> SAM modified surfaces. This analysis also verifies that similar Faradaic efficiencies between different modified surfaces are due inherently to the intended catalyst and not due to experimental error.

It is interesting to note in all three voltages that all three azide-terminated SAMs



**Figure 25:** Molar CO yields of different porphyrin modified surfaces (a,b) and charge comparisons of each porphyrin modified surface (c,d).

produce modest amount of CO (Figure 23a, b, c, red lines) despite not being CO<sub>2</sub> reactive.

This could be due to the electron tunneling of the SAMs still causing components of the FTO to reduce from oxidized tin to tin metal and allowing exposed metal to catalytically

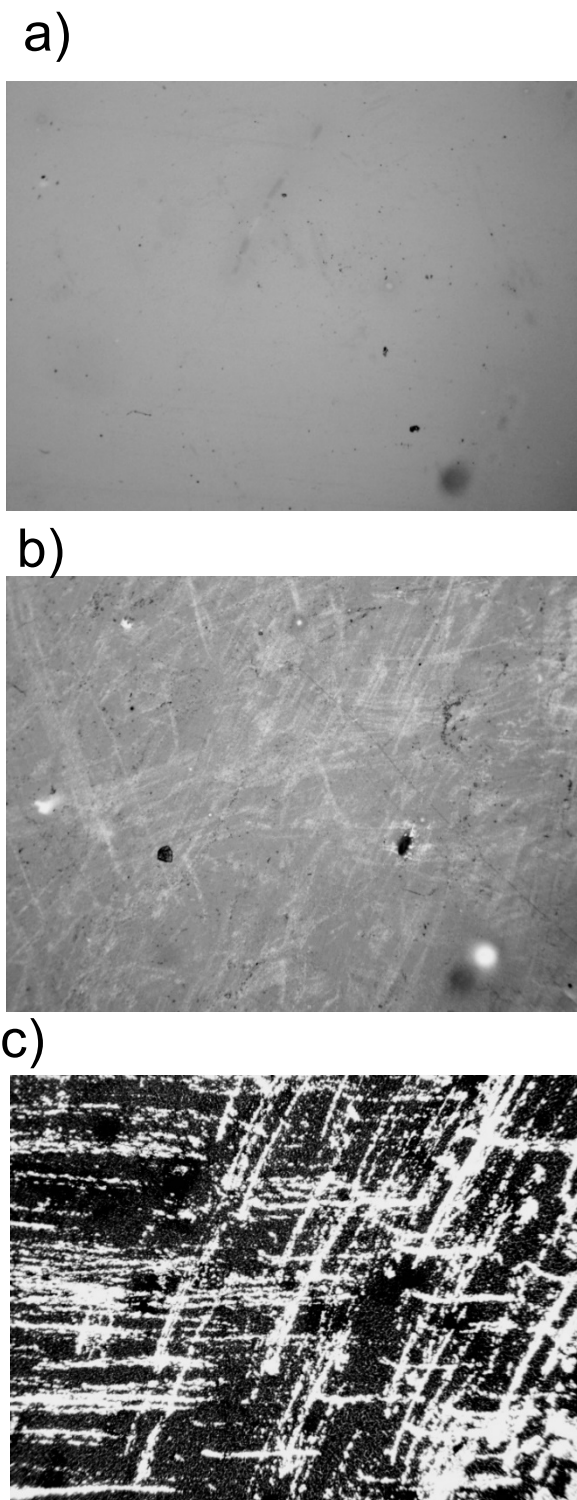


**Figure 26:** Optical microscope images at medium objective for porphyrin modified FTO surfaces after experiment at -1.2 V (a), -1.4 V (b) and -1.6 V (c).

facilitate  $\text{CO}_2$  reduction. Pictures from optical microscopy at the three different voltages after chronoamperometry support this hypothesis showing greater degradation (dark areas, rough morphology) of the surface through higher voltages (Figure 26). If true, co-catalysis could always be occurring to some degree at each voltage between reduced tin and the porphyrins, and further testing could confirm this as well as to what extent each is contributing.

Chronoamperometry was again carried out with continuous flow of  $\text{CO}_2$  at -1.6 V, -1.4 V and -1.2 V for 1 hour with  $\text{C}_{11}$  and  $\text{C}_5$  azide-terminated SAM lengths to determine formate production. Interestingly, the trend is reversed for all three voltages compared to CO faradaic efficiencies, showing a depression at -1.4 V and higher yields present at -1.2 V and -1.6 V for all surfaces (Figure 27a). FeTPP shows the highest Faradaic efficiency of

the porphyrins at -1.6 V at 28.6%, however CoTPP has the highest yield of 22.9% at -1.2 V. Both results fall in line with the hypothesis of isomerization of the CO<sub>2</sub> molecule during metal bonding. At a higher potential, FeTPP produces more formate resulting from sufficient thermodynamics and isomerization of CO<sub>2</sub>, while at a lower potential, CoTPP produces more formate. The thermodynamics for FeTPP at -1.2 V not being enough for isomerization or even cleavage of the metal – CO<sub>2</sub> bond. C<sub>5</sub> SAM modified CoTPP surfaces (Figure 27b) show little formate production, similar to amounts of CO production, due to excessively fast electron kinetics.

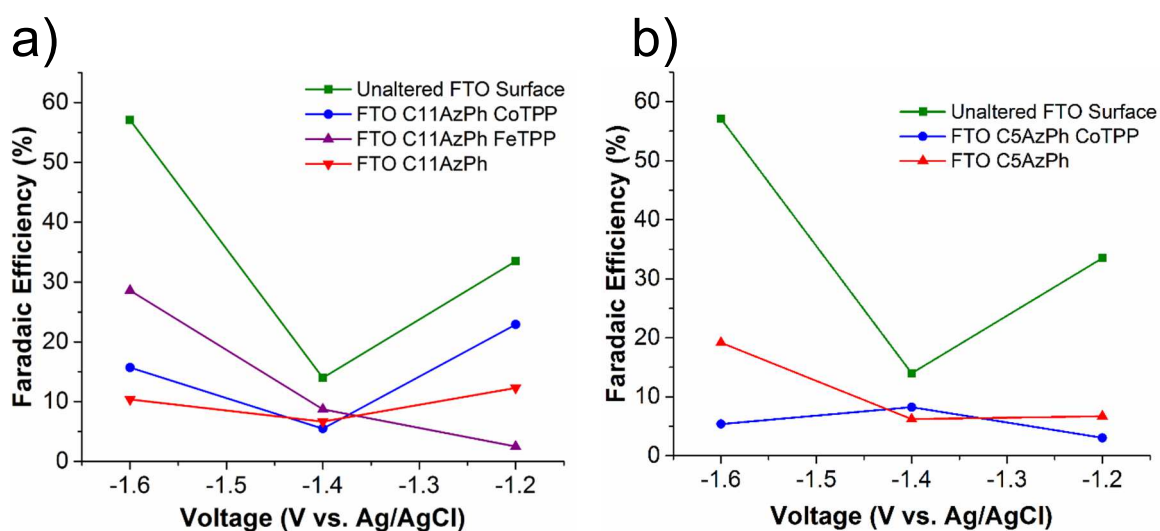


**Figure 27:** Faradaic efficiencies at three voltages for C<sub>11</sub> SAM (a) and C<sub>5</sub> SAM (b).

The reason for the selectivity difference of Co versus Fe may also arise from the metal's  $\pi$ -donor ability as postulated for Co and Fe complexes of another N-containing macrocycle.[17] In both metals, CO<sub>2</sub> initially bonds via the carbon atom, however with the electron rich Co atom,  $\pi$  back-bonding weakens the C-O bond making cleavage easier and more readily produces CO. In contrast, the Fe atom is a poorer  $\pi$ -donor, and isomerization of the bound CO<sub>2</sub> occurs more readily, effectively producing more formate. Oxophilicity

and  $\pi$ -donor ability synergistically help explain experimental results presented here. Figure 28 summarizes the Faradaic efficiency results explained in this thesis.

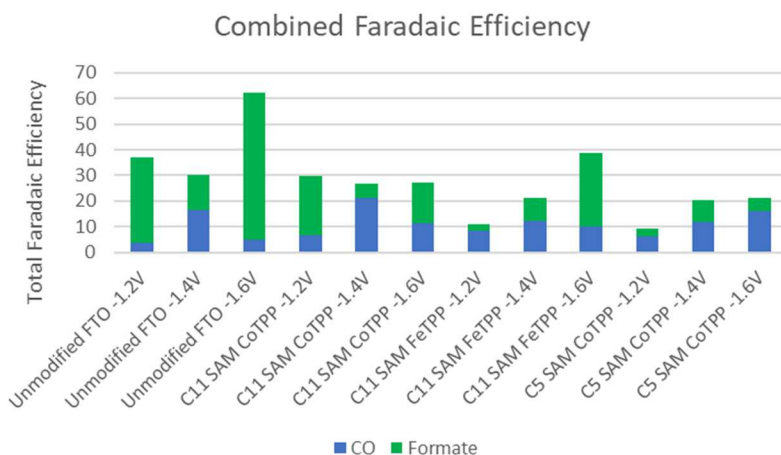


**Figure 28:** Combined Faradaic efficiencies for CoTPP and FeTPP porphyrin modified surfaces with C<sub>11</sub> and C<sub>5</sub> SAMs.

#### 4. Conclusions

We formed SAMs of Fe and Co porphyrins on Au and ITO electrodes using azide-alkyne click chemistry. Although the SAMs on Au electrodes catalyze the O<sub>2</sub> reduction reaction, these electrodes are not compatible with CO<sub>2</sub> reduction potentials. Therefore, we constructed analogous SAMs on ITO electrodes that are more electrochemically stable to facilitate CO<sub>2</sub> reduction. Through preliminary experiments it was determined FTO would be a more suitable substrate, so we also formed C<sub>5</sub>, C<sub>11</sub> and C<sub>16</sub> SAMs of Fe and Co porphyrins on FTO electrodes. To discern patterns of electrocatalytic behavior among the porphyrins three chronoamperometry experiments at -1.2 V, -1.4 V and -1.6V were examined for each architecture. Electrochemical experiments and AFM images confirm the presence of porphyrins on the electrodes. Although both Fe and Co porphyrins generate H<sub>2</sub>, the Fe porphyrin is usually more selective towards formate production while the Co porphyrin favors CO production. While many other homogeneous CO<sub>2</sub> reduction catalysts

win in selectivity and Faradaic efficiency, they lack in tunability and control. This work lays a foundation for future work studying porphyrins or other CO<sub>2</sub> reduction catalysts using a highly tunable clickable SAM architecture and shows the possibilities available to control electron kinetics via suitable substrates and SAMs to improve Faradaic yield.

## References

- [1] R. Kunzig, **Climate Milestone: Earth's CO<sub>2</sub> Level Passes 400 ppm**, National Geographic, 2019.
- [2] Y. Hori, K. Kikuchi, S. Suzuki, **Production of carbon monoxide and methane in electrochemical reduction of carbon dioxide at metal electrodes in aqueous hydrogen carbonate solution** Chem. Lett., 14 (1985), 1695-1698
- [3] Y. Hori, A. Murata, R. Takahashi, **Formation of hydrocarbons in the electrochemical reduction of carbon dioxide at a copper electrode in aqueous solution** J. Chem. Soc., Faraday Trans. 1, 85 (1989), 2309-2326
- [4] Q. Lu, J. Rosen, Y. Zhou, G.S. Hutchings, Y.C. Kimmel, F. Jiao, J.G. Chen, **A selective and efficient electrocatalyst for carbon dioxide reduction** Nat Commun, 5 (2014), 3242
- [5] S. Gao, Y. Lin, X. Jiao, Y. Sun, Q. Luo, W. Zhang, D. Li, J. Yang, Y. Xie, **Partially oxidized atomic cobalt layers for carbon dioxide electroreduction to liquid fuel** Nature (London, U. K.), 529 (2016), 68-71
- [6] Q. Lu, J. Rosen, F. Jiao, **Nanostructured metallic electrocatalysts for carbon dioxide reduction** ChemCatChem, 7 (2015), 38-47
- [7] Y. Hori, **Electrochemical CO<sub>2</sub> reduction on metal electrodes** Mod. Aspects Electrochem., 42 (2008), 89-189
- [8] Y. Chen, M.W. Kanan, **Tin Oxide Dependence of the CO<sub>2</sub> Reduction Efficiency on Tin Electrodes and Enhanced Activity for Tin/Tin Oxide Thin-Film Catalysts** J. Am. Chem. Soc., 134 (2012), 1986-1989
- [9] D. Ren, Y. Deng, A.D. Handoko, C.S. Chen, S. Malkhandi, B.S. Yeo, **Selective Electrochemical Reduction of Carbon Dioxide to Ethylene and Ethanol on Copper(I) Oxide Catalysts** ACS Catal., 5 (2015), 2814-2821
- [10] J. Qiao, Y. Liu, F. Hong, J. Zhang, **A review of catalysts for the electroreduction of carbon dioxide to produce low-carbon fuels** Chem. Soc. Rev., 43 (2014), 631-675
- [11] S.N. Supakul, C.J. Barile, **Membrane-modified metal triazole complexes for the electrocatalytic reduction of oxygen and carbon dioxide** Front. Chem. (Lausanne, Switz.), 6 (2018), 543
- [12] J.P. Collman, N.K. Devaraj, T.P.A. Eberspacher, C.E.D. Chidsey, **Mixed Azide-Terminated Monolayers: A Platform for Modifying Electrode Surfaces** Langmuir, 22 (2006), 2457-2464
- [13] C.C.L. McCrory, A. Devadoss, X. Ottenwaelder, R.D. Lowe, T.D.P. Stack, C.E.D. Chidsey, **Electrocatalytic O<sub>2</sub> Reduction by Covalently Immobilized Mononuclear**

- Copper(I) Complexes: Evidence for a Binuclear Cu<sub>2</sub>O<sub>2</sub> Intermediate** *J. Am. Chem. Soc.*, 133 (2011), 3696-3699
- [14] C.E.D. Chidsey, **Free Energy and Temperature Dependence of Electron Transfer at the Metal-Electrolyte Interface** *Science*, 251 (1991), 919-922
- [15] J.P. Collman, N.K. Devaraj, R.A. Decréau, Y. Yang, Y.-L. Yan, W. Ebina, T.A. Eberspacher, C.E.D. Chidsey, **A Cytochrome c Oxidase Model Catalyzes Oxygen to Water Reduction Under Rate-Limiting Electron Flux** *Science*, 315 (2007), 1565-1568
- [16] B.-X. Dong, S.-L. Qian, F.-Y. Bu, Y.-C. Wu, L.-G. Feng, Y.-L. Teng, W.-L. Liu, Z.-W. Li, **Electrochemical Reduction of CO<sub>2</sub> to CO by a Heterogeneous Catalyst of Fe-Porphyrin-Based Metal-Organic Framework** *ACS Appl. Energy Mater.*, 1 (2018), 4662-4669
- [17] L. Chen, Z. Guo, X.-G. Wei, C. Gallenkamp, J. Bonin, E. Anxolabehere-Mallart, K.-C. Lau, T.-C. Lau, M. Robert, **Molecular Catalysis of the Electrochemical and Photochemical Reduction of CO<sub>2</sub> with Earth-Abundant Metal Complexes. Selective Production of CO vs HCOOH by Switching of the Metal Center** *J. Am. Chem. Soc.*, 137 (2015), 10918-10921
- [18] Z. Weng, J. Jiang, Y. Wu, Z. Wu, X. Guo, K.L. Materna, W. Liu, V.S. Batista, G.W. Brudvig, H. Wang, **Electrochemical CO<sub>2</sub> Reduction to Hydrocarbons on a Heterogeneous Molecular Cu Catalyst in Aqueous Solution** *J. Am. Chem. Soc.*, 138 (2016), 8076-8079
- [19] L. Angnes, E.M. Richter, M.A. Augelli, G.H. Kume, **Gold Electrodes from Recordable CDs** *Analytical Chemistry*, 72 (2000), 5503-5506
- [20] J. Nakazawa, B.J. Smith, T.D.P. Stack, **Discrete Complexes Immobilized onto Click-SBA-15 Silica: Controllable Loadings and the Impact of Surface Coverage on Catalysis** *J. Am. Chem. Soc.*, 134 (2012), 2750-2759
- [21] P. Tao, A. Viswanath, L.S. Schadler, B.C. Benicewicz, R.W. Siegel, **Preparation and Optical Properties of Indium Tin Oxide/Epoxy Nanocomposites with Polyglycidyl Methacrylate Grafted Nanoparticles** *ACS Appl. Mater. Interfaces*, 3 (2011), 3638-3645
- [22] R.P. Gautam, Y.T. Lee, G.L. Herman, C.M. Moreno, E.C.M. Tse, C.J. Barile, **Controlling Proton and Electron Transfer Rates to Enhance the Activity of an Oxygen Reduction Electrocatalyst** *Angew. Chem., Int. Ed.*, 57 (2018), 13480-13483
- [23] D. Wechsler, M. Franke, Q. Tariq, L. Zhang, T. Lee, P.K. Thakur, N. Tsud, S. Bercha, K.C. Prince, H. Steinruck, O. Lytken, **Adsorption Structure of Cobalt Tetraphenylporphyrin on Ag(100)** *J. Phys. Chem. C*, 121 (2017) 5667-5674
- [24] K. Sengupta, S. Chatterjee, A. Dey, **Catalytic H<sub>2</sub>O<sub>2</sub> Disproportionation and Electrocatalytic O<sub>2</sub> Reduction by a Functional Mimic of Heme Catalase: Direct Observation of Compound 0 and Compound I in Situ** *ACS Catal.*, 6 (2016), 1382-1388
- [25] A. Hosseini, C.J. Barile, A. Devadoss, T.A. Eberspacher, R.A. Decreau, J.P. Collman, **Hybrid Bilayer Membrane: A Platform To Study the Role of Proton Flux on the Efficiency of Oxygen Reduction by a Molecular Electrocatalyst** *J. Am. Chem. Soc.*, 133 (2011), 11100-11102
- [26] F. Rollet, S. Morlat-Thérias, J.-L. Gardette, **AFM analysis of CD-R photoaging** *Polym. Degrad. Stab.*, 94 (2009), 877-885

- [27] L. Srisombat, A.C. Jamison, T.R. Lee, **Stability: A key issue for self-assembled monolayers on gold as thin-film coatings and nanoparticle protectants** *Colloids Surf., A*, 390 (2011), 1-19
- [28] O. Yildirim, M.D. Yilmaz, D.N. Reinhoudt, D.H.A. Blank, G. Rijnders, J. Huskens, **Electrochemical Stability of Self-Assembled Alkylphosphate Monolayers on Conducting Metal Oxides** *Langmuir*, 27 (2011), 9890-9894
- [29] N.M. Berezina, M.I. Bazanov, A.A. Maksimova, A.S. Semeikin, **Electrochemical behavior of meso-substituted iron porphyrins in alkaline aqueous media** *Russ. J. Phys. Chem. A*, 91 (2017), 2377-2382
- [30] N. Araki, M. Obata, A. Ichimura, Y. Amao, K. Mitsuo, K. Asai, S. Yano, **Redox and photochemical behaviour of a porphyrin monolayer on an indium-tin oxide electrode** *Electrochim. Acta*, 51 (2005), 677-683
- [31] A. Brisach-Wittmeyer, S. Lobstein, M. Gross, A. Giraudeau, **Electrochemical reduction of 1-(meso-tetraphenylporphyrin)-pyridinium cations** *J. Electroanal. Chem.*, 576 (2005), 129-137
- [32] D. Raoufi, Z. Kalali, **Wavelet-fractal approach to surface characterization of nanocrystalline ITO thin films** *Phys. B (Amsterdam, Neth.)*, 407 (2012), 4369-4374
- [33] C.-Y. Li, T.-C. Wen, T.-F. Guo, S.-S. Hou, **A facile synthesis of sulfonated poly(diphenylamine) and the application as a novel hole injection layer in polymer light emitting diodes** *Polymer*, 49 (2008), 957-964
- [34] K.P. Kuhl, E.R. Cave, D.N. Abram, T.F. Jaramillo, **New insights into the electrochemical reduction of carbon dioxide on metallic copper surfaces** *Energy Environ. Sci.*, 5 (2012), 7050-7059
- [35] Bard, A. J., Parsons, R., and Jordan, J. **Standard Potentials in Aqueous Solutions** Marcel Dekker, New York, 1985
- [36] K. P. Kepp. **A Quantitative Scale of Oxophilicity and Thiophilicity** *Inorg. Chem.* 55 (2016), 9461-9470